ANL-ART-166

Development of the Technical Basis of a Unified Viscoplastic Model of 316H Stainless Steel for Incorporation into ASME Division 5

Applied Materials Division

ANL-ART-166

Development of the Technical Basis of a Unified Viscoplastic Model of 316H Stainless Steel for Incorporation into ASME Division 5

Applied Materials Division
Argonne National Laboratory

July 2019

Prepared by

M. C. Messner, Argonne National Laboratory
V.-T. Phan, Argonne National Laboratory
T.-L. Sham, Argonne National Laboratory

Abstract

This report describes the development of a unified viscoplastic model describing the deformation of 316 stainless steel. The model was developed for incorporation into Section III, Division 5 of the ASME Boiler and Pressure Vessel Code covering the design and fabrication of Class A high temperature nuclear reactor components. The current version of the Code does not provide reference inelastic models, leaving the responsibility of defining an adequate model up to either the plant owner or designer. This approach represents a substantial barrier to using the ASME design by inelastic analysis methods. As historical practice demonstrates these methods produce much more efficient designs, compared to the design by elastic analysis methods, eliminating this barrier could result in safer, more effective, and more efficient structural designs thereby lowering the cost of future advanced reactors. This report summarizes the process of gathering experimental data, calibrating the candidate inelastic model against that data, and validating the model. The report also summarizes work on a new method of calculating the sensitivities of history dependent nonlinear constitutive models that was used to calibrate the 316H model using gradient-based optimization.

Table of Contents

List of Figures

List of Tables

1 Introduction

1.1 Objectives

This report describes the process of calibrating and validating an inelastic deformation model for 316H stainless steel suitable for use with the ASME Section III, Division 5, Subsection HB, Subpart B design by inelastic analysis rules. The ultimate goal of this work is to incorporate the model in the ASME Code as being acceptable for use with the design by inelastic analysis provisions. Currently, the Code does not provide a reference material model for 316H (or any other material), instead leaving the specification of the inelastic model to either the Owner/Operator in the Design Specification or the design as part of the Design Report. This approach imposes a substantial barrier to the use of the inelastic methods, as the designer must first calibrate or locate a sufficiently accurate constitutive model. Past work as part of the Clinch River Breeder Reactor Project (CRBRP) demonstrates that the design by inelastic analysis methods are the least overconservative and therefore their use leads to most efficient, most economical design [9]. Indeed, the CRBRP found it necessary to apply the inelastic design methods to certain critical reactor components in order to demonstrate the safety of the design – the elastic design methods were too conservative to produce feasible designs at these key locations [9].

A suitable model for 316H must fulfill the requirements stated in the Code, described in the next section. Additionally, a companion report describes an extension to the rather limited guidance provided in the 2019 edition of the Code aimed at more clearly defining which aspects of the material's constitutive response are critical to capture for design with the Code.

1.2 Model requirements

The current Code in HBB-3214.2 requires that the inelastic model captures the details of creep and plasticity in the material at high temperatures, including any effect of

- Strain and cyclic hardening or softening
- The interaction of creep with plasticity and vice-versa
- Primary creep deformation and its interaction with strain hardening.

A companion report describes an extension of this limited guidance, which is briefly summarized here.

The Code uses the constitutive response predicted by the material model in two ways. First, it uses the accumulated strain at the end of the component service life as an acceptability criterion to guard against ratcheting. This means the model must accurately predict long-term creep deformation, at least up to the Code acceptability criteria of 5% accumulated strain, as well as ratcheting under general cyclic loading. Secondly, the Code uses the service cycle strain ranges and stress relaxation profiles to predict creep-fatigue damage. This means the material model must accurately predict cyclic inelastic deformation, even though the model need not explicitly represent damage as the damage calculation is done with a separate Code procedure.

Previous work has demonstrated that above a certain threshold temperatures, established to be 740° C for 316H, a non-unified model decomposing inelastic deformation into separate rate-independent plasticity and rate-dependent creep contributions become unsuitable as creep and plasticity cannot be distinguished [10, 11]. In this temperature regime a unified viscoplastic model is more appropriate.

The Code requires the model represent an average, not a minimum, material response. For the purposes of this material model, which is supposed to generically encompass all 316H material allowed for high temperature use by the Code, the model should therefore capture the average response of all heats of 316H material. The experimental database summarized in Chapter 2 demonstrates a wide scatter in material properties, even for material that meet the 316H material specification. This poses a substantial challenge to fitting an adequate model, as described in greater detail below.

Finally, the model should accurately represent deformation under the multiaxial stress states found in actual components. This is a challenge as test data is nearly always collected using uniaxial samples. Instead, the model developed here is extended from 1D to 3D using standard flow theory. Ideally, a few multiaxial tests would be used to validate these assumptions, however such test data is not available for 316H.

1.3 Organization of the report

The report is divided into three main sections. Chapter 2 describes the experimental database used to calibrated the inelastic model. This database pulls together records of tests from available literature data into a common format. This chapter summarizes the types and sources of data and describes the scatter and average response contained in the data set. Chapter 3 describes the process used to develop the model and calibrated it to the data. This chapter describes the development of a new, efficient way to optimize models using gradient-based optimization and a novel, efficient method of computing the model sensitivities. The chapter concludes by tabulating the final, recommended set of material properties. Chapter 4 then describes the process used to validate the final model against the experimental data. Chapter 5 summarizes the work done as part of this project and lays out the process required to get the model adopted as part of the ASME Code. Appendix A provides the Code language to be used to ballot the model to the relevant ASME Code Committees.

2 Experimental database

To support the development of the model a large experimental database was collated from the open literature and experimental databases. Data collection efforts focused on four types of common experiments:

1. Monotonic strain controlled tension tests, of the type defined in the ASTM E21 standard [12] but including tests run at non-standard strain rates. These experiments load a uniaxial sample in strain-controlled monotonic tension at a constant strain rate and temperature. The measured data is a flow curve plotting strain versus stress (see Fig. 2.1 for an example). These flow curves are commonly reported in the literature. These experiments measure the initial flow stress (yield stress), ultimate tensile stress, and work hardening characteristics of the material. However, monotonic tests are not sufficient to distinguish isotropic from kinematic hardening (see Chapter 3).

2. Creep tests. These tests hold a uniaxial sample at a constant tensile stress for a long period of time at a fixed, elevated temperature. For the test data collected here the result of the experiment is a creep curve plotting accumulated creep strain versus time, which can be post-processed into a plot of creep strain rate versus time (see Fig. 2.2 for an example). Creep tests can be used to constrain the material's long-term rate dependent deformation, including the effect of hardening or softening on the flow rate.

3. Stress relaxation tests hold the uniaxial sample at a fixed strain and measure the stress as a function of time at constant temperature. The direct measurement is a stress relaxation curve plotting the current flow stress through time (see Fig. 2.3). This type of test directly measures the material's stress relaxation behavior.

4. Creep-fatigue tests, otherwise known as strain-controlled cyclic tests. These experiments cycle a uniaxial test specimen through some strain-controlled, cyclic load history. The test keeps the temperature fixed. Holds may be incorporated into the cycle during which the sample is held at constant strain. Commonly, this load history is defined by a maximum value of tensile strain, the load ratio between the minimum strain values and the maximum strain value, hold times applied at either the maximum or minimum strain value, the loading strain rate, and the fixed temperature. This type of test most directly mimics the loading experienced by a component in service. This type of test samples the entire constitutive response of the material and provides the data required to distinguish isotropic from kinematic hardening. However, strain controlled tests usually have short hold times so that the total test time to failure remains relatively short and therefore these experiments must be supplemented the with creep tests to capture the material's long-term behavior. The direct experimental output of these tests is a series of (time,strain,stress) points that can be plotted to form stress-strain hysteresis loops (Fig. 2.4a) or a stress-time relaxation history (Fig. 2.4b). However, the time history cannot be extracted from plotted hysteresis loops because the loops overlap and more commonly experimentalists report only the maximum and minimum stress as a function of cycle count (Fig. 2.4c). Therefore, this report deals only with these cycle summary information as that is all that is available for the majority of the tests.

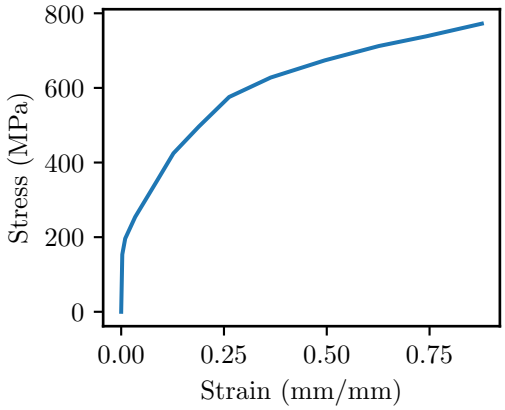

Figure 2.1: Example uniaxial flow curve from reference [1]. Test was conducted at 550° C.

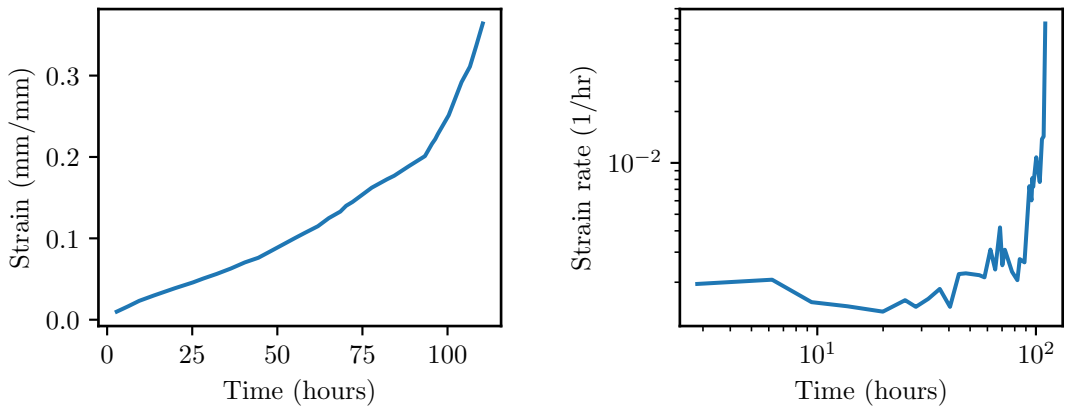

(a) (b)

Figure 2.2: Sample creep data from [2] at 650° C and an applied stress of 207 MPa. (a) plots the data as a creep curve showing creep strain versus time. (b) plot the same data as a creep rate curve, plotting the creep strain rate versus time. The noise in the rate data comes from numerically differentiating the measured creep strain data.

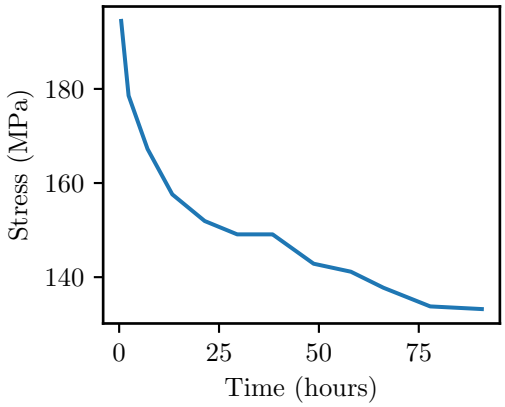

Figure 2.3: Sample stress relaxation data from [1] at 600° C with an applied strain of 2.0%.

Field	Description	Example
source	Text description of data source	ORNL (1974)
specimen	Sample geometry details, if provided by the source	0.875-inch gauge-length specimen
control	Stress or strain controlled test	strain
testtype	Description of loading type, currently only uniaxial	uniaxial
direction	Direction of loaded for textured samples	RD
tc	Tension or compression loading	tension
rate	Strain rate of loading	0.0004
temperature	Test temperature	298.15
stress	Stress points along flow curve	0,10.2,20.5,...
strain	Strain points along flow curve	0,0.001,0.002,0.003,...
time	Time points along flow curve	0,1,2,3,...
youngs	Calculated Young's modulus	180000
yield	Calculated yield stress (0.02% offset)	281.0

Table 2.1: Data recorded for uniaxial tension tests.

Tables 2.1, 2.2, and 2.3 record the experimental data and metadata recorded for each experiment of a given type. The metadata can be used to sort material by type and experiments by source. The data is stored in an XML format so the entire database can be easily searched and queried. Units are stored as XML attributes. A postprocessing script converts the data to the unit system used to fit the model: megapascals for stress, seconds for time, nominal strains, and Kelvin for temperature.

Table 2.4 summarizes the number of test records and corresponding sources from the open literature collected for calibrating the inelastic model.

A critical compromise had to be made in collecting this data: not all of the tested material meets the 316H material specification. There was insufficient data on 316H material to constrain a model for the entire required temperature range. This decision likely contributes to the experimental scatter observed in the data, summarized below. While the scope of the data collection effort was expanded beyond 316H it was not expanded to encompass 316L

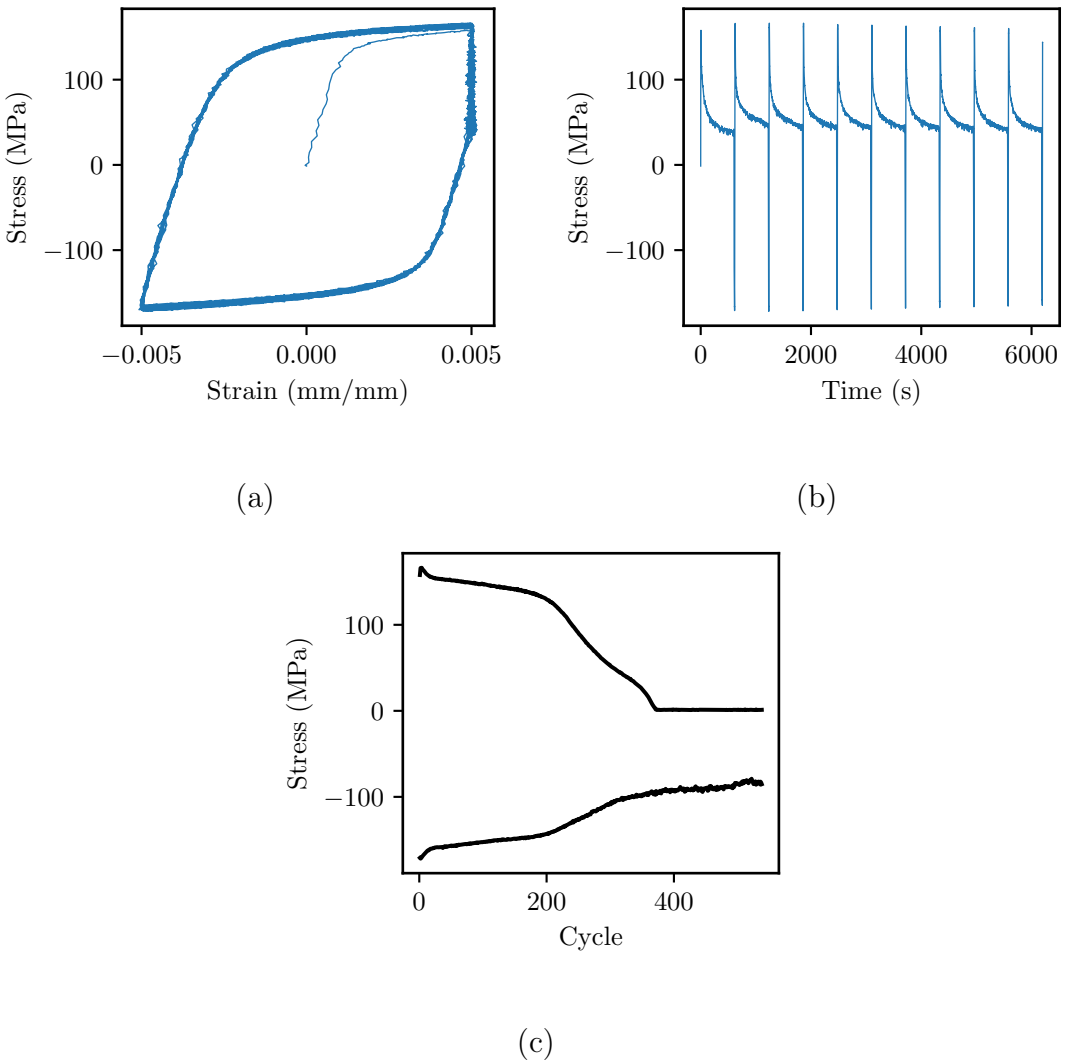

Figure 2.4: Sample creep-fatigue test data from [3]. Test conditions are full-reversed loading through a 1% strain range, a 10 minute hold on the tensile end of the cycle, and at 815° C. (a) plots stress-strain hysteresis loops and (b) plots the stress/time history for the first 10 cycles. (c) plots the maximum and minimum stress recorded for each cycle for the full test. The data in (c) is what is most commonly reported in the literature.

Field	Description	Example
source	Text description of data source	ORNL (1974)
specimen	Sample geometry details, if provided by the source	0.875-inch gauge-length specimen
control	Stress: creep test; strain: stress relaxation test	strain
testtype	Description of loading type, currently only uniaxial	uniaxial
direction	Direction of loaded for textured samples	RD
tc	Tension or compression loading	tension
rate	Applied loading rate	0.0004
temperature	Test temperature	298.15
value	Applied stress (creep) or strain (relaxation)	120
relax	Measured strain (creep) or stress (relaxation)	0,1,2,3,...
relaxrate	Measured strain rate (creep) or stress rate (relaxation)	100,100,200,300,...
time	Time points along relaxation curve	0,1,2,3,...

Table 2.2: Data recorded for creep and stress relaxation tests.

Field	Description	Example
source	Text description of data source	ORNL (1974)
specimen	Sample geometry details, if provided by the source	0.875-inch gauge-length specimen
control	Stress or strain controlled test	strain
testtype	Description of loading type, currently only uniaxial	uniaxial
direction	Direction of loaded for textured samples	RD
rate	Strain rate of loading	0.0004
temperature	Test temperature	298.15
value	Maximum value of strain or stress	0.005
ratio	R-ratio: max value / min value of applied load	-1.0
hold	Hold time: attribute provides “max” “min” or “both”	3600
stress	Recorded stress data (optional)	0,10.2,20.5,...
strain	Recorded strain data (optional)	0,0.001,0.002,0.003,...
time	Recorded time data (optional)	0,1,2,3,...
cycle	cycle count	1,2,3,4,...
min	Minimum value of stress or strain as a function of cycle count	-100,-120,-130,...
max	Maximum value of stress or strain as a function of cycle count	50,60,70,...

Table 2.3: Data recorded for cyclic tests.

Source	Material	Tensile	Creep	Stress relaxation	Creep-fatigue	Temperature range (°C)
Sikka et al. (1980) [2]	316H	124	18	0	0	25 to 760
Kanazawa and Yoshida (1974) [13]	316	0	0	0	22	25 to 700
Ohno et al. (1998) [14]	316FR	6	0	0	0	650
Hyde (1997) [15]	316	0	10	0	0	550 to 600
Mohanty et al. (2016) [16]	316	0	0	0	6	20 to 300
Fookes et al. (2009) [17]	316H	0	0	4	0	550
Albertini et al. (1991) [18]	316	2	0	0	0	20
Hammond and Sikka (1976) [19]	316H	22	0	0	0	24 to 316
Takahashi, Shibamoto, and Inoue (1997) [20]	316FR	4	1	0	28	25 to 600
Horak, Sikka, and Raske (1983) [21]	316H	0	2	0	0	593
Zhu, Boerman, and Piatti (1983) [22]	316H	0	32	0	0	426 to 721
Mizuno (2000) [23]	316FR	6	0	0	0	25
Yoon et al. (2015) [24]	316H	0	0	0	9	25 to 650
Wood et al. (1987) [25]	316H	2	0	0	1	400
Hyde (1986) [26]	316	0	5	0	0	550
Whittaker, Evans, and Wilshire (2012) [27]	316H	0	2	0	0	550 to 700
DeSisto and Carr (1961) [28]	316H	6	0	0	0	-195 to 0
Hormozi, Biglari, and Nikbin (2015) [29]	316FR	0	0	3	3	650
Youtsos, Donea, and Verzeletti (1989) [30]	316H	8	0	0	0	25
Yoshida et al. (1997) [31]	316FR	7	0	0	1	25 to 650
Kim et al. (2008) [1]	316	0	0	1	0	600
Other DOE reports and databases	316H	6	0	0	4	25 to 650
Totals	*Grand total: 345*	*193*	*70*	*8*	*74*	

Table 2.4: Sources of experimental data from the open literature used to calibrate the model.

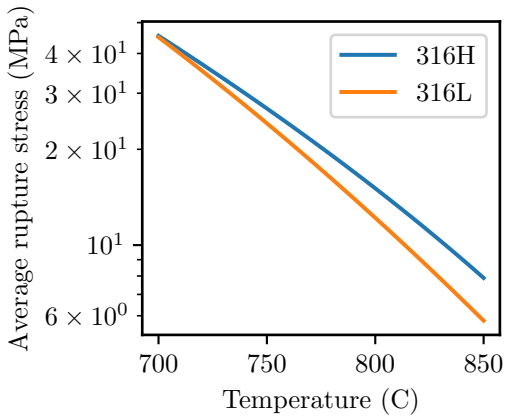

Figure 2.5: Comparison between the rupture stress for 316H (from the Larson-Miller correlation in [4]) and 316L (from a Larson-Miller correlation fit by the authors to data from [5, 6]) for 100,000 hours life.

material. 316H has a signficantly better creep rupture life at temperatures above 700° C, as evidenced by the comparison plotted in Fig. 2.5. However, the collection effort did include 316, 316H, and 316FR material. Table 2.5 compares the chemical compositions of these three materials. All 316H and 316FR material meets the 316 specification, but not all 316 material meets the 316H or 316FR specification.

Table 2.5 also shows the recommended chemical composition limits for 316H recommended by the current version of the ASME Boiler and Pressure Vessel Code Section III, Division 5 [32] providing design rules for high temperature nuclear components. These suggested chemistry limits are tighter than the base material specification. Many test summaries do not include the exact composition of the material and it is in any event unlikely that most of the tested 316H material meets these additional guidelines with the exception of recent tests conducted by the DOE. Furthermore, the Code requires 316H material pass a creep-fatigue acceptance test defined in Section III, Division 5, Subsection HB, Subpart B, HBB-2800. Again, it is unlikely that this acceptance test was performed for the bulk of the material, with the exception of tests performed by the DOE.

All this variation in material chemistry produces a large variation in material properties. Figure 2.6 plots the recorded yield stress data for the entire database as a function of temperature. Overlaid on the plot are the ASME Code values of S_y, which correspond to the minimum allowable yield strength at room temperature, and a line trending through the average yield stress at each temperature. The scatter in the measured data is obvious. Some of this scatter is caused by allowable composition variations within the 316H and some of the variation is caused by material processing, for example bar versus plate data. However, the bulk is likely due to the inclusion of non-316H data in the database. While there is a large scatter about the mean, none of the data fails to meet the minimum specified room temperature yield strength for 316H, which is identical to the ASME value of S_y at room temperature. This means that, at least for this single material property, all of this material meets the 316H specification.

Material	Limit	Cr	Ni	Mo	C	Mn	P	S	Si	N
316	Min	16	10	2						
	Max	18	14	3	0.08	2.00	0.045	0.03	0.75	0.1
316FR	Min	16	10	2			0.020			0.06
	Max	18	14	3	0.02	2	0.045	0.03	1.00	0.12
316H	Min	16	10	2	0.04					
	Max	18	14	3	0.10	2	0.045	0.03	0.75	
316H, ASME suggested	Min	17	11	2.5	0.04	1				0.04
	Max	18	12.5	3	0.06	2	0.03	0.02	0.60	0.07

Table 2.5: Comparison of the composition specification for 316, 316FR, 316H, and the current suggested 316H chemistry from Nonmandatory Appendix HBB-U of Section III, Division 5 of the ASME Code. The ASME recommended composition also contains additional restrictions on trace elements. All entries are in wt%. Blank entries mean the applicable limit is not specified. The balance of the material composition is Fe. Composition of 316FR referenced in [8].

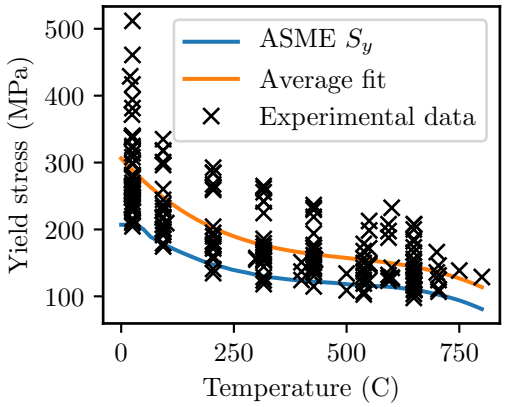

Figure 2.6: Yield stress data from the complete experimental database, plotted as a function of temperature. Overlaid on the data are two trend lines: the ASME design value of yield strength S_y and a best-fit polynomial. This plot includes data collected at all strain rates.

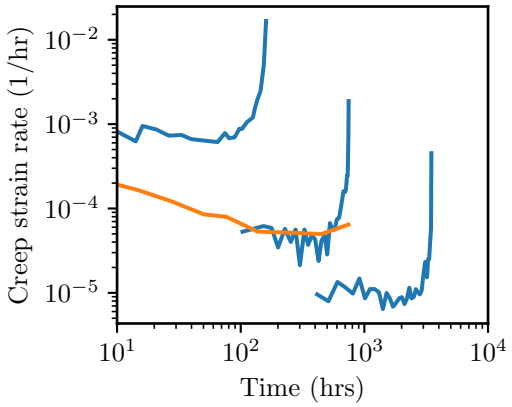

Figure 2.7: Example of typical scatter in creep data. These four creep curves represent four tests at the same experimental conditions of applied load 276 MPa and temperature 650° C. The experiments plotted in blue are all from the same source [2] and tested at the same lab. The experiment plotted in orange is from [7].

Similarly, Fig. 2.7 plots four creep curves from the experimental database all at the same experimental conditions of an applied load of 276 MPa at a test temperature of 650° C. The three curves plotted in blue are from the same source [2] and may be taken as representative of the heat-to-heat variation for 316H material tested in the same laboratory on the same equipment. Scatter in measured creep properties is typical, even for material within the 316H composition specification, but including the additional material likely contributes additional scatter. A similar variation in the cyclic response should be expected, though the database contains very few replicate tests at the same conditions that can be used to visually demonstrate the expected variation.

The variation in the available test data produces a difficult problem in calibrating an inelastic model. The ASME Code guidance for design by inelastic analysis suggest the model should match the average response of all 316 stainless steel meeting the Class A Code requirements. However, even the Code's relatively restricted composition range will produce a large variation in material properties. Fitting a model to capture the average response of data with such scatter is a challenging optimization problem. Furthermore, validating the model against experimental data is extremely difficult as an average-property model is exceedingly unlikely to reproduce the response of a particular test which is essentially a single random sample of the property distribution. Chapter 4 discusses the process adopted to validate the model in greater detail.

3 Model form and calibration

3.1 Previous models

There is relatively little past work on modeling 316H material. The only complete inelastic constitutive model for 316H suitable for high temperature use identified in the literature is the "ORNL model" developed as part of the Clinch River Breeder Reactor Project (CRBRP) at Oak Ridge National Laboratory. A Welding Research Council Bulletin [9] summarizes the development of this model, which is also documented in the literature [33, 34, 35, 36, 37]. This model was used to design critical components for the CRBRP and so was, at least at the time, deemed suitable for use with the ASME method of design by inelastic analysis. However, the model fundamentally relies on heuristic methods of accounting for creep-plasticity interactions (the α-reset procedures and β-option) and uses a cycle-counting algorithm to represent changes in the material's kinematic hardening response. These features make the model unsuitable for modern design with FEA.

Several partial models for 316H exist. Youtsos et al. provide a model for the monotonic rate sensitivity of 316H [30] but do not address the cyclic or creep response of the material. Gong et al. provide a viscoplastic Chaboche model for 316 [38], which is the model form used in this report. However, they did not consider the creep deformation of the material, for example they use a constant rate sensitivity exponent of $n = 10$ across a wide temperature range. Additionally, their model was calibrated to a single set of experimental data on a single heat and is therefore not suitable for generic use with the ASME Code. Tokuda et al. provide a complete, non-unified model for 316H [39]. As discussed in the introduction, non-unified models are unsuitable for 316H at very high temperatures. More fundamentally, this paper does not provide a complete description of the model sufficient to reproduce their results. Chaboche himself has provided various models for 316 steel (c.f. [40]) but these models only cover a limited temperature range and a single heat of material.

There is also a great deal of modeling work on 316L steel, which is the commercially more common material (for example see [41, 42, 43, 44]). However, this work cannot be applied to 316H. As demonstrated in the previous chapter, the high temperature properties of 316L differ greatly from 316H. Therefore, the remainder of this report details the process of calibrating a new model for 316H suitable for use with the ASME design by inelastic method and validating the model against test data.

3.2 Model selection

The form selected for the inelastic model must be capable of representing the key deformation features identified in the introduction:

- Strain and cyclic hardening or softening
- Primary creep and creep strain hardening or softening
- The effect of creep on plasticity and vice-versa.

Though the model will be calibrated to relatively short-term data, the constitutive representation should reasonably extend to the low stress, long time deformation regime expected

for in-service reactor components. There are numerous suitable model forms, for example those developed by Ohno and Wang [45, 46] and Krempl [47, 48, 49]. However, the mostly widely-adopted model is the Chaboche formulation [50, 51, 52, 53, 54, 55, 56], which is implemented in a wide variety of engineering finite element analysis software. Therefore, this report targets calibrating a Chaboche model to the data set described in the previous chapter.

The full unified viscoplastic Chaboche formulation captures the interaction of creep and plasticity at high temperatures, and therefore the report adopts this variant of the general model. The model is presented in the context of small strains, but can be extended to large deformations using standard methods. The model divides the total strain rate into elastic, viscoplastic, and thermal contributions

$$\dot{\boldsymbol{\varepsilon}} = \dot{\boldsymbol{\varepsilon}}_e + \dot{\boldsymbol{\varepsilon}}_{vp} + \dot{\boldsymbol{\varepsilon}}_{th}. \tag{3.1}$$

The stress rate relates linearly to the elastic strain rate

$$\dot{\boldsymbol{\sigma}} = \boldsymbol{C} : \dot{\boldsymbol{\varepsilon}}_e \tag{3.2}$$

where $\boldsymbol{C}$ is a temperature-dependent isotropic elasticity tensor defined by the Young's modulus E and Poisson's ratio ν. The thermal strain is proportional to the temperature rate through the temperature-dependent instantaneous thermal expansion coefficient

$$\dot{\boldsymbol{\varepsilon}}_{th} = \alpha \dot{T} \mathbf{I}. \tag{3.3}$$

In the model both the elastic properties and the coefficient of thermal expansion are not fit to data but rather set the values provided in Section II, Part D of the ASME Code [57].

The viscoplastic strain rate is defined by a power law flow rule

$$\dot{\boldsymbol{\varepsilon}}_{vp} = \sqrt{\frac{3}{2}} \left\langle \frac{f\left(\boldsymbol{\sigma} - \boldsymbol{X}\right) - \sigma_0 - \sqrt{\frac{2}{3}} R}{\sqrt{2/3}\eta} \right\rangle^n \frac{\partial f}{\partial \boldsymbol{\sigma}} \tag{3.4}$$

where $\boldsymbol{X}$ is the kinematic backstress, σ_0 is a threshold stress, R is the isotropic hardening, and η and n are temperature-dependent parameters describing the material's rate sensitivity. The model uses a J_2 flow rule so that

$$f\left(\boldsymbol{\sigma}\right) = \sqrt{\frac{3}{2} \operatorname{dev}\left(\boldsymbol{\sigma}\right) : \operatorname{dev}\left(\boldsymbol{\sigma}\right)} \tag{3.5}$$

where the dev operator takes the deviatoric part of a tensor.

The evolution of the isotropic hardening follows the Voce model

$$\dot{R} = b\left(Q - R\right) \dot{\bar{\varepsilon}}_{vp} \tag{3.6}$$

where b and Q are temperature-dependent material parameters and $\dot{\bar{\varepsilon}}_{vp}$ is the equivalent inelastic strain rate

$$\dot{\bar{\varepsilon}}_{vp} = \sqrt{\frac{3}{2}} \left\langle \frac{f\left(\boldsymbol{\sigma} - \boldsymbol{X}\right) - \sigma_0 - \sqrt{\frac{2}{3}} R}{\sqrt{2/3}\eta} \right\rangle^n . \tag{3.7}$$

The full form of the Chaboche kinematic hardening model, including static recovery, is

$$\boldsymbol{X} = \sum_{i=1}^{n_{back}} \boldsymbol{X}_i \tag{3.8}$$

$$\dot{\boldsymbol{X}}_i = \left(\frac{2}{3} C_i \frac{\partial f}{\partial \boldsymbol{\sigma}} - \sqrt{\frac{2}{3}} \gamma_i \boldsymbol{X}_i \right) \dot{\bar{\varepsilon}}_{vp} - A_i \sqrt{\frac{3}{2}} f \left(\boldsymbol{X}_i \right)^{a_i - 1} \boldsymbol{X}_i \tag{3.9}$$

where n_{back} is the number of backstresses and C_i, γ_i, A_i, and a_i are temperature-dependent parameters. A preliminary analysis of the data suggested that two backstresses were sufficient to capture the observed cyclic behavior. Additional sensitivity analysis show that the available data does not constrain the static recovery parameters A_i and a_i. This does not mean that the response of a single, consistent sample of the material would not exhibit static recovery or require more than two backstresses, but rather that the scatter in the data makes distinguishing these fine details of the constitutive response impossible. Therefore, the form used here neglects the static recovery terms and sets $n_{back} = 2$.

The complete model supplements the Chaboche model for inelastic deformation with a Hayhurst-Leckie-Kachanov [58, 59] model for creep damage. The intent of including this damage model is not to accurately model creep rupture but rather to capture the accelerating creep rate during the onset of tertiary creep. This modification means the final model is defined by the integration the rate equation

$$\dot{\boldsymbol{\sigma}} = (1 - \omega) \boldsymbol{C} : (\dot{\boldsymbol{\varepsilon}} - \dot{\boldsymbol{\varepsilon}}_{vp} - \dot{\boldsymbol{\varepsilon}}_{th}) \tag{3.10}$$

which is a rearrangement of Eqs. 3.1 and 3.2 supplemented by the damage variable ω. The preceding equations defining inelastic flow and the evolution of the model's internal history are supplemented this equation for the stress rate and the damage evolution equation

$$\dot{\omega} = \frac{\left(\frac{f(\boldsymbol{\sigma})}{A} \right)^{\chi}}{(1 - \omega)^{\phi}} \tag{3.11}$$

where A, χ, and ϕ are temperature-dependent parameters.

The model was calibrated at discrete temperatures with an interpolation scheme providing the parameter values in between the calibration temperatures. One set of temperatures — 25°, 550°, 600°, 650°, and 700° C — was selected to encompass the bulk of the test conditions in the database. Two additional temperatures — 427° and 815° C — were added to capture the start of the creep range and the maximum use temperature for 316H for Section III of the ASME Code. Not counting the fixed elastic constants and the coefficient of thermal expansion there are 12 parameters to calibrate at each temperature and so the model has 84 parameters to fit. The next section describes the process of calibrating these parameters to the experimental database.

3.3 Calibrating models with gradient-based optimizer

3.3.1 Background

Past work on the Grade 91 inelastic model used genetic algorithm optimization (GA) to fit model parameters to the available experimental data [60, 61, 62]. Genetic algorithm opti-

mization is a heuristic that attempts to find a global optima, that is the best possible fit between the model and the data. While this is the ultimate objective in fitting a constitutive model, GA is a heuristic and so sensitive to the meta-parameters used to tune the optimization method and the particular choice of GA features [63]. Additionally, GA optimization requires a large number of forward model evaluations. Because time integration cannot be parallelized, this makes the approach extremely costly when fitting cyclic plasticity models.

An alternative to GA optimization are a wide category of gradient-based optimization techniques [64, 65]. These methods do not attempt to find a global optima, but instead seek a local optimal point. However, they are not heuristics and can be shown to be guaranteed to achieve local optima, provided the objective function and constraints meet certain conditions. Applying a gradient-based optimizer to the model calibration problem discussed previously will produce a good result in the sense of a local minima but not necessarily the best possible set of parameters. Past experience with GA-fit material models shows that the process requires extensive manual intervention. This is not necessarily a problem, provided the final model can be successfully validated against experimental data. However, gradient-based methods, if they can be applied to the problem, have the advantage that the result of the process is at least a local optima and therefore is mathematically at least a local best-fit.

Applying gradient-based methods requires the problem sensitivity: the derivative of the objective function with respect to the model parameters. Conceptually, the objective function used to fit the constitutive models takes the form

$$o\left(\boldsymbol{p}\right) = \sum_{experiments} \left(\frac{\text{model} - \text{experiment}}{\text{experiment}} \right)^2, \tag{3.12}$$

that is the square of the relative error (RSE) between the predicted model response for a given set of parameters $\boldsymbol{p}$ and the corresponding experimental measurements. This objective function is formalized for the different test types below. The sensitivity is then the derivative of the objective function with respect to the parameters

$$\boldsymbol{g} = \frac{do}{d\boldsymbol{p}}. \tag{3.13}$$

Given Eq. 3.12, calculating the sensitivity of the constitutive modeling problem requires the derivative of the model response with respect to the model parameters. This would either be the derivative of the strain history with respect to the parameters

$$\boldsymbol{m}_{\sigma i} = \frac{d\varepsilon_i}{d\boldsymbol{p}} \tag{3.14}$$

for stress-controlled tests or the derivative of the stress history with respect to the parameters

$$\boldsymbol{m}_{\varepsilon i} = \frac{d\sigma_i}{d\boldsymbol{p}} \tag{3.15}$$

for strain-controlled tests.

These derivatives are difficult to calculate for the complex, nonlinear, history-dependent constitutive model defined in Section 3.2. One option might be to use a finite-difference

scheme to calculate the sensitivity. This would require $1 + |\boldsymbol{p}|$ evaluations of the model for each experiment, where $|\boldsymbol{p}|$ is the number of parameters, instead of the single evaluation required to evaluate the objective function. The cost of these extra evaluations is prohibitive for cyclic experiments. A single model evaluation for a cyclic test requires a large amount of non-parallizable computer time to execute because the load history on the sample must be tracked with multiple integration time steps and each cycle must be explicitly modeled. Experience with the constitutive model used here shows that about 50 steps are required to load, hold, and unload the model in each cycle. The total required number of steps is then $N_t = 50N_{cycles}$ where N_{cycles} is the number of load cycles in the test. For a typical creep-fatigue test with 500 load cycles to failure this represents 25,000 integration steps through the constitutive model. This computational cost cannot be parallelized, as it represents time integration.

The second challenge in computing the constitutive model sensitivities is that the model used here is history dependent. This means that the model response at the current time step depends on the model response at all previous time steps. Similarly, the current value of the sensitivity depends not just on the current input but also on the past input. Applying a gradient-based optimization method to calibrating the constitutive model described here requires a new, numerically-efficient method for computing the problem sensitivity.

3.3.2 A method for computing the exact sensitivities of history-dependent constitutive models

3.3.2.1 General framework

Consider a time series of data defined by a set of tuples

$$\mathcal{H}_i = \{\boldsymbol{x}_i, \boldsymbol{y}_i, \boldsymbol{f}_i\} \tag{3.16}$$

where the time series is given by a recursive, implicit nonlinear function defined such that

$$\boldsymbol{x}_{i+1} = \mathcal{F}\left(\boldsymbol{x}_{i+1}, \boldsymbol{x}_i, \boldsymbol{y}_{i+1}, \boldsymbol{y}_i, \boldsymbol{f}_{i+1}, \boldsymbol{p}\right). \tag{3.17}$$

We will call the time series of vectors $\boldsymbol{x}_i$ the "forward state," the time series of vectors $\boldsymbol{y}_i$ the "backward state," the time series of vectors $\boldsymbol{f}_{i+1}$ the "given state," and the (constant) vector $\boldsymbol{p}$ the model parameters. We are interested in finding

$$\boldsymbol{S}_{\boldsymbol{x}} = \left.\frac{d\boldsymbol{x}_{i+1}}{d\boldsymbol{p}}\right|_{\boldsymbol{y}_{i+1}} \tag{3.18}$$

the sensitivity of the forward state with respect to the parameters for fixed backward state.

Assume we have solved for $\boldsymbol{x}_{i+1}$ such that

$$\boldsymbol{R}_{i+1} = \boldsymbol{x}_{i+1} - \mathcal{F}\left(\boldsymbol{x}_{i+1}, \boldsymbol{x}_i, \boldsymbol{y}_{i+1}, \boldsymbol{y}_i, \boldsymbol{f}_{i+1}, \boldsymbol{p}\right) = \boldsymbol{0} \tag{3.19}$$

and assume $\mathcal{F}$ is adequately differentiable. In practice this solution is provided by Newton's method, or a variant thereof, applied to a backward Euler integration of the model rate equations.

By the implicit function theorem

$$d\boldsymbol{R}_{i+1} = \frac{\partial \boldsymbol{R}_{i+1}}{\partial \boldsymbol{x}_{i+1},} : d\boldsymbol{x}_{i+1} + \frac{\partial \boldsymbol{R}_{i+1}}{\partial \boldsymbol{x}_i} : d\boldsymbol{x}_i + \frac{\partial \boldsymbol{R}_{i+1}}{\partial \boldsymbol{y}_{i+1}} : d\boldsymbol{y}_{i+1} + \frac{\partial \boldsymbol{R}_{i+1}}{\partial \boldsymbol{y}_i} : d\boldsymbol{y}_i + \frac{\partial \boldsymbol{R}_{i+1}}{\partial \boldsymbol{f}_{i+1},} : d\boldsymbol{f}_{i+1} + \frac{\partial \boldsymbol{R}_{i+1}}{\partial \boldsymbol{p}} : d\boldsymbol{p} = \boldsymbol{0} \quad (3.20)$$

$$\frac{\partial \boldsymbol{R}_{i+1}}{\partial \boldsymbol{x}_{i+1},} : \frac{d\boldsymbol{x}_{i+1}}{d\boldsymbol{p}} + \frac{\partial \boldsymbol{R}_{i+1}}{\partial \boldsymbol{x}_i} : \frac{d\boldsymbol{x}_i}{d\boldsymbol{p}} + \frac{\partial \boldsymbol{R}_{i+1}}{\partial \boldsymbol{y}_{i+1}} : \frac{d\boldsymbol{y}_{i+1}}{d\boldsymbol{p}} + \frac{\partial \boldsymbol{R}_{i+1}}{\partial \boldsymbol{y}_i} : \frac{d\boldsymbol{y}_i}{d\boldsymbol{p}} + \frac{\partial \boldsymbol{R}_{i+1}}{\partial \boldsymbol{f}_{i+1},} : \frac{d\boldsymbol{f}_{i+1}}{d\boldsymbol{p}} + \frac{\partial \boldsymbol{R}_{i+1}}{\partial \boldsymbol{p}} = \boldsymbol{0}. \quad (3.21)$$

the backward and the given state is fixed

$$\frac{\partial \boldsymbol{R}_{i+1}}{\partial \boldsymbol{x}_{i+1},} : \frac{d\boldsymbol{x}_{i+1}}{d\boldsymbol{p}} + \frac{\partial \boldsymbol{R}_{i+1}}{\partial \boldsymbol{x}_i} : \frac{d\boldsymbol{x}_i}{d\boldsymbol{p}} + \frac{\partial \boldsymbol{R}_{i+1}}{\partial \boldsymbol{p}} = \boldsymbol{0}. \quad (3.22)$$

Define

$$\boldsymbol{J}_{i+1} = \frac{\partial \boldsymbol{R}_{i+1}}{\partial \boldsymbol{x}_{i+1}}. \quad (3.23)$$

Note that

$$\boldsymbol{x}_{i+1} = \boldsymbol{x}_i + \Delta \boldsymbol{x}_{i+1} \quad (3.24)$$

or

$$\boldsymbol{x}_{i+1} - \boldsymbol{x}_i - \Delta \boldsymbol{x}_{i+1} = \boldsymbol{0} = \boldsymbol{R}_{i+1} \quad (3.25)$$

$$\frac{\partial \boldsymbol{x}_{i+1}}{\partial \boldsymbol{x}_i} - \frac{\partial \boldsymbol{x}_i}{\partial \boldsymbol{x}_i} - \frac{\partial \Delta \boldsymbol{x}_{i+1}}{\partial \boldsymbol{x}_i} = \boldsymbol{0} = \frac{\partial \boldsymbol{R}_{i+1}}{\partial \boldsymbol{x}_i} \quad (3.26)$$

with $\frac{\partial \Delta \boldsymbol{x}_{i+1}}{\partial \boldsymbol{x}_i} = \boldsymbol{0}$ then

$$\frac{\partial \boldsymbol{R}_{i+1}}{\partial \boldsymbol{x}_i} = -\boldsymbol{I}. \quad (3.27)$$

Then

$$\boldsymbol{J}_{i+1} : \frac{d\boldsymbol{x}_{i+1}}{d\boldsymbol{p}} - \frac{d\boldsymbol{x}_i}{d\boldsymbol{p}} + \frac{\partial \boldsymbol{R}_{i+1}}{\partial \boldsymbol{p}} = \boldsymbol{0}. \quad (3.28)$$

And so

$$\frac{d\boldsymbol{x}_{i+1}}{d\boldsymbol{p}} = \boldsymbol{J}_{i+1}^{-1} : \left(\frac{d\boldsymbol{x}_i}{d\boldsymbol{p}} - \frac{\partial \boldsymbol{R}_{i+1}}{\partial \boldsymbol{p}} \right). \quad (3.29)$$

Equation 3.29 provides a recursive update formula for calculating $\boldsymbol{S}_{\boldsymbol{x}}$, now dropping the subscript $\boldsymbol{x}$

1. Start with $\boldsymbol{S}_0 = \boldsymbol{0}$.
2. After solving for state $i+1$ update $\boldsymbol{S}_{i+1} = \boldsymbol{J}_{i+1}^{-1} : \left(\boldsymbol{S}_i - \frac{\partial \boldsymbol{R}_{i+1}}{\partial \boldsymbol{p}} \right)$.

3.3.2.2 Standard constitutive models

The general framework can be applied to constitutive models of the type defined in Section 3.2.

Identify the forward state as

$$\boldsymbol{x} = \{\boldsymbol{\sigma}, \boldsymbol{h}\} \tag{3.30}$$

the stress and internal history variables; the backward state as

$$\boldsymbol{y} = \{\boldsymbol{\varepsilon}\} \tag{3.31}$$

the strain; and the given state as

$$\boldsymbol{f} = \{T, t\} \tag{3.32}$$

the temperature and time; and $\boldsymbol{p}$ the model parameters. Equation 3.29 provides a method for calculating the sensitivity of the stresses (or strains) with respect to the model parameters. Moreover, in the case of implicit time integration with Newton's method it is a numerically efficient method. Suppose our stress update formula is given by an implicit integration of a set of coupled ordinary differential equations solved with Newton's method:

$$\boldsymbol{x}_{i+1} = \boldsymbol{x}_i + \dot{\boldsymbol{x}}\left(\boldsymbol{x}_{i+1}, \boldsymbol{x}_i, \boldsymbol{y}_{i+1}, \boldsymbol{y}_i, \boldsymbol{f}_{i+1}, \boldsymbol{p}\right) \tag{3.33}$$

$$\boldsymbol{R}_{i+1}^{(j)} = \boldsymbol{x}_{i+1}^{(j)} - \boldsymbol{x}_i^{(j)} - \dot{\boldsymbol{x}}\left(\boldsymbol{x}_{i+1}^{(j)}, \boldsymbol{x}_i^{(j)}, \boldsymbol{y}_{i+1}, \boldsymbol{y}_i, \boldsymbol{f}_{i+1}, \boldsymbol{p}\right) \tag{3.34}$$

$$\boldsymbol{x}_{i+1}^{(j+1)} = \boldsymbol{x}_{i+1}^{(j)} - \boldsymbol{J}_{i+1}^{(j)-1} : \boldsymbol{R}_{i+1}^{(j)} \tag{3.35}$$

then we can identify $\boldsymbol{J}_{i+1}$ as the Jacobian required to determine the material update using Newton's method for the last, converged iteration:

$$\boldsymbol{J}_{i+1} = \boldsymbol{J}_{i+1}^{(j)} \text{ if } \boldsymbol{R}_{i+1}^{(j)} = \boldsymbol{0}. \tag{3.36}$$

This means we already have the inverse calculated in the course of a normal stress update. The only new information needed to calculate the sensitivities is the partial derivative $\frac{\partial \boldsymbol{R}_{i+1}}{\partial \boldsymbol{p}}$. These are the partial derivatives of the constitutive model with respect to the model parameters. For example, if the stress update is defined as

$$\boldsymbol{\sigma}_{n+1} = K \operatorname{tr}\left(\boldsymbol{\varepsilon}_{n+1}\right) \boldsymbol{I} + 2G\left(\boldsymbol{\varepsilon}_{n+1} - \frac{1}{3}\operatorname{tr}\left(\boldsymbol{\varepsilon}_{n+1}\right) \boldsymbol{I}\right) \tag{3.37}$$

then for parameter set $\boldsymbol{p} = \{K, G\}$ the required partials are

$$\frac{\partial \boldsymbol{R}}{\partial K} = -\operatorname{tr}\left(\boldsymbol{\varepsilon}_{n+1}\right) \boldsymbol{I} \tag{3.38}$$

$$\frac{\partial \boldsymbol{R}}{\partial G} = -2\left(\boldsymbol{\varepsilon}_{n+1} - \frac{1}{3}\operatorname{tr}\left(\boldsymbol{\varepsilon}_{n+1}\right) \boldsymbol{I}\right). \tag{3.39}$$

These partials are generally easy to calculate even for more sophisticated constitutive models.

This section specialized the generic method, presented above, to a strain-controlled problem where the input is strain, temperature, and time, and the output is the stress and the model history. A similar derivation can be used to find the sensitivities for a stress-controlled problem where the input is stress, temperature, and time and the output is strain.

3.3.3 Implementation of the method

This generic methodology was implemented in a python code called "pyoptmat." The software contains 1D implementations of the unified viscoplastic Chaboche model, described above, as well as other standard high temperature constitutive models. The framework applies the method described here to calculate the sensitivities of the models for generic stress or strain-controlled load histories. In general, the implementations are standard backward Euler implicit integrations of the standard model rate-form equations. However, the framework also calculates and maintains the required model partial derivatives with respect to the parameters, which are not often implemented in constitutive modeling software.

In addition to the models, the software package contains methods for managing experimental data, running instances of a model through load histories representing the standard test types described in Chapter 2 and computing the corresponding sensitivities, and methods for running a model through fully-defined strain-temperature-time or stress-temperature-time histories, the type of data, for example, that is measured directly in a creep-fatigue test before post-processing into maximum/minimum stress versus cycle count plots. Additional details on the objective functions used for the standard experiments are provided below.

The software integrates the IPOPT solver [66] to optimize the model parameters with respect to some set of experimental data. The optimizer accommodates bounds on the parameter values so that the model parameters can be constrained to physical values. For example, in all the optimization problems discussed here the model rate sensitivity n is constrained to be greater than one, based on physical arguments, and less than 20, as values greater than 20 return essentially the same nearly rate-independent response and yet make the integration of the equations much more difficult.

3.3.4 Tests on synthetic data

As an example to demonstrate the utility of the gradient-based optimization approach consider the simple model defined by the parameters given in mean value column in Table 3.1. The model uses simple linear isotropic and kinematic hardening, as opposed to the full Chaboche form used for the 316H model. The mathematical, uniaxial description of the model is

$$\dot{\sigma} = E\left(\dot{\varepsilon} - \dot{\varepsilon}_{vp}\right) \tag{3.40}$$

$$\dot{\varepsilon}_{vp} = \left(\frac{\langle |\sigma - Q| - \sigma_0 - R \rangle}{\eta}\right)^n \tag{3.41}$$

$$\dot{Q} = H\dot{\varepsilon}_{vp} \tag{3.42}$$

$$\dot{R} = K\left|\dot{\varepsilon}_{vp}\right|. \tag{3.43}$$

To provide a benchmark optimization problem, a series of "synthetic experiments" were run by simulating standard strain controlled cyclic tests with randomly-generated loading parameters drawn uniformly from the ranges shown in Table 3.2. All the synthetic tests repeat the loading cycle five times. Figure 3.1 plots one of these synthetic experiments both as a stress-strain hysteresis loop and a stress-time history. This set of synthetic experiments

Parameter	Description	Lower bound	Mean/fixed value	Upper bound
E	Young's modulus	n/a	150000	n/a
σ_0	Threshold stress	n/a	0	n/a
n	Rate sensitivity	1	10	20
η	Viscosity	15	150	1500
K	Isotropic hardening modulus	100	1000	10,000
H	Kinematic hardening modulus	200	2000	20,000

Table 3.1: Parameters used to generate the synthetic data. The table shows the mean value of the parameter distribution used to generate the synthetic data (for $COV = 0.0$ the exact parameters used to generate the data) and the upper and lower limits applied to each parameter during optimization. Bounds values of "n/a" indicate that this parameter (the Young's modulus and the threshold stress) were not optimized but rather fixed to the mean value.

was then used to refit the model to match the data starting from randomly generated initial parameters drawn from the ranges shown in Table 3.1. The optimization problem solved was

$$\begin{aligned} \min \; o(\boldsymbol{p}) \text{ such that} & \\ p_i \leq & \quad p_i^{(ub)} \\ p_i \geq & \quad p_i^{(lb)} \end{aligned} \tag{3.44}$$

and

$$o(\boldsymbol{p}) = \sum_{i=1}^{n_{test}} \sum_{j=1}^{n_i} \left(\hat{\sigma}_i(\boldsymbol{p}) - \sigma_i\right)^2 \tag{3.45}$$

where n_{test} are the number of tests, n_i is the number of load steps in test i, $\hat{\sigma}_i(\boldsymbol{p})$ is the model stress response on step i to a load history defined by a time series of strains, temperatures, and times and σ_i is the corresponding stress in the synthetic experiment. Table 3.1 shows the bounds applied to each parameter, which are the same as the range used to sample the random initial parameters. These bounds are quite nonrestrictive for the most part extending one order of magnitude above and below the parameters used to generate the synthetic data. The exception is the rate sensitivity exponent which was limited to be between 1 (a physical constraint on standard rate sensitivity) and 20 (a numerical constraint to prevent a stiff response).

Figure 3.1 plots the results of applying the method to this synthetic problem, providing the optimizer 10 randomly-generated synthetic experiments. The figure shows three sets of stress-strain hysteresis loops for one of the randomly-generated load history: the synthetic experimental data, the model predictions with the initial, random parameters, and the optimized model response. The method exactly recovers the input constitutive response, demonstrating the gradient-based method work efficiently, at least for consistent, synthetic experimental data. These results are repeatable: in five trials with initially random parameters the optimizer always recovered the exact parameter set used to generate the data (within reasonable round-off error). A parametric study shows that the optimizer performs with this same efficiency when provided with only a single synthetic experiment, albeit at the expense of requiring additional optimization iterations to find a solution.

Parameter	Description	Lower limit	Upper limit
ε_{max}	Maximum strain	0.0	0.05
R	Loading ratio (max/min strain)	-1.0	1.0
$\dot{\varepsilon}$	Strain rate	10^{-6}	10^{0}
t_{max}	Hold at maximum strain	0	10,000
t_{min}	Hold at minimum strain	0	10,000

Table 3.2: The loading parameters for the strain controlled cyclic synthetic experiments were drawn uniformly from the bounds shown in this table with the exception of the strain rate which was sampled log-uniformly.

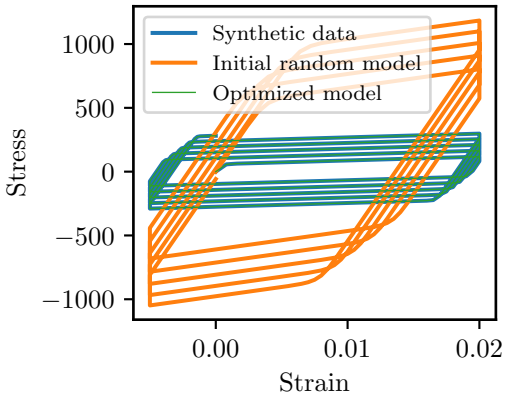

Figure 3.1: Results from models initialized with three sets of parameters for a random strain controlled loading: the reference parameters used to generate the synthetic data, an initially, randomly selected set of parameters drawn from Table 3.1, and the final, optimized parameter set (which falls directly on top of the synthetic data).

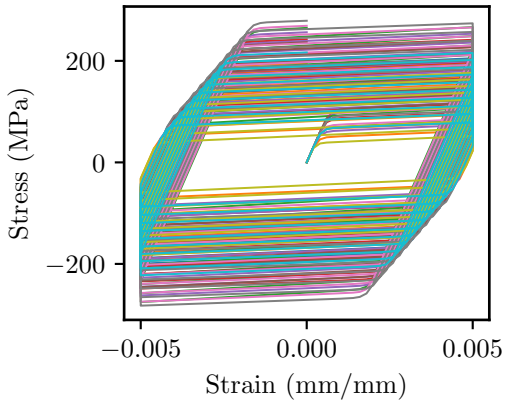

Figure 3.2: Example of the variation in random samples of the standard model with a coefficient of variation of 0.2. The loading conditions are fully-reversed strain-controlled loading with a strain range of 1%, a loading rate of 10^{-3}/s, a tension hold of 1 hour and a compression hold of 0.5 hours.

Of course, as discussed in Chapter 2, real experimental data does not draw from a single set of material properties. Instead the properties a single material, as defined by a composition specification, range through a potentially wide distribution. A second set of reference optimization problems was developed to assess the gradient-based optimization method for a statistical distribution of measured material properties. The framework is the same as the problem with perfect synthetic data, but now the random synthetic experiments both select random loading conditions (drawn from Table 3.2) and random properties for the synthetic material. Each trial selects each property from uncorrelated normal distributions centered about the mean properties in Table 3.1 with a standard deviation described by a parameterized coefficient of variation $COV = \mu/\sigma$ where μ is the property mean value and σ the standard deviation. Several cases were considered with $COV = 0.1$, 0.2, and 0.3. Figure 3.2 shows the scatter in synthetic material response for the $COV = 0.2$ case by plotting the results of 10 random selections from the property distributions all for the same loading conditions, noted in the figure caption.

3.4 Model calibration

The 316H material model was calibrated using the gradient-based method described in Section 3.3, fit against the experimental database described in Chapter 2. There are several additional challenges that needed to be overcome to apply the method to real data.

The first challenge is the form of the residual. Fundamentally, all types of experiments use the RSE metric defined in Eq. 3.12. For uniaxial tension, creep, and stress relaxation tests the application of this metric is straightforward. For each individual test and set of model parameters $\boldsymbol{p}$ the process is:

1. Use the experiment metadata to simulate the experiment using the model defined by parameters $\boldsymbol{p}$. For each type of test:

(a) Uniaxial: simulate a strain controlled flow curve at the appropriate rate and temperature.

(b) Creep: simulate a constant-stress test by loading the model up to the experimental stress at the experimental loading rate and temperature and holding at fixed stress for the full experimental time.

(c) Stress relaxation: simulate a constant strain test by loading the model up to the experimental strain at the experimental rate and temperature and holding at fixed strain for the full experimental time.

2. Extract data from the model to compare to the test

   (a) Uniaxial: the full stress/strain flow curve.

   (b) Creep: the creep strain versus time data for the hold at constant stress.

   (c) Stress relaxation: the stress versus time relaxation profile during the hold at constant strain.

3. Determine the RSE for the test by calculating

$$RSE = \sum_{i=1}^{n_{test}} \left(\frac{m_i - e_i}{e_i} \right)^2 \tag{3.46}$$

   where m_i is the model prediction and e_i is the experimental value and the sum proceeds over each point along the relevant curve (flow curve, creep curve, or stress relaxation curve).

The cyclic test are handled differently. The challenge is that the common experimental result is the maximum and minimum stress for each cycle, for a strain controlled test, or the maximum and minimum strain, for a stress controlled test. Calculating the maximum stress over a cycle from the model results does not represent a differentiable function, which means the sensitivity cannot be calculated. Instead, the procedure used in the fit process replaces the hard maximum or minimum with an appropriate p-norm. The process then becomes:

1. Use the experiment metadata to simulate the experiment using the model defined by parameters $\boldsymbol{p}$. Specifically, simulate a strain or stress controlled cyclic test, as appropriate, with the experimental maximum value, R-ratio, loading rate, and hold times.

2. Extract the complete stress/strain/time data from the model along with brackets indicating which portion of this history corresponds to which loading cycle.

3. Calculate the error

$$RSE = \sum_{i=1}^{n_{cycle}} \left(\frac{\left\| m_j \middle| \, j \in C_i \right\|_p - e_i}{e_i} \right)^2 \tag{3.47}$$

   where e_i is the experimental cycle max or min data, m_j are the model predicted stress (strain-control) or strain (stress-control) values, C_i is the set of indices j that comprise

load cycle i, $\|\|\|_p$ is an appropriate p-norm to replace either the hard minimum or maximum, and the sum proceeds over each cycle recorded in the experiment. After some numerical testing we found that $p = 60$ adequately replaces the hard maximum operator without causing numerical instability.

Applying this process to each experiment in the fit database produces a series of errors, one for each test. These errors must be combined to form the total objective function minimized by the optimizer. This process necessarily involves selecting heuristic weights for each experiment. These weights are currently set by the user based on engineering judgment on which types of test data are most important for the final model to accurately capture.

The optimization process to generate the final 316H model proceeded incrementally. The entire process was completed for each temperature individually so that the model results are calibrated for discrete temperatures and interpolated, as described below. For a given temperature first the deformation parameters — n, η, σ_0, b, Q, C_1, γ_1, C_2, and γ_2 with E, ν, and α fixed to the ASME values — were calibrated to the experimental data using the optimization process described above. The weights for each experiment where kept constant within a class – i.e. all uniaxial tests shared the same weight, all creep tests shared a different weight, etc. These weights were calibrated heuristically by first generating a good guess at the model parameters for the temperature of interest and determining the initial value of the objective function for each type of experiment – all the uniaxial tests, all the creep tests, all the relaxation tests, and all the cyclic tests. Call these initial category residuals c_k. The weight for each class of test was set to

$$w_k = \frac{r_k}{c_k} \tag{3.48}$$

where r_k was 1.0 for creep, stress relaxation, and uniaxial tests and 2.0 for cyclic tests. This process approximately neutralizes the differences in the magnitude of the error between the different types of results and then weights the cyclic tests higher than the monotonic tests. This process was developed based on our judgment that the cyclic response is more important to high temperature engineering design than the monotonic response.

The Chaboche parameters are not unique . Different combinations of the backstress parameters can all produce the same stress/strain/time response. However, for the final model ideally the temperature-dependent parameters would fall along a more-or-less smooth curve to simplify temperature interpolation. In order to achieve this result we first fit the model parameters at 600° C where a large amount of experimental data was available. The initial guess for this optimization run was selected based on manual tuning. After successfully optimizing the parameters at 600° C this set of parameters was used as the initial guess for optimizing the 550° and 650° C parameters. This process was repeated up and down the temperature range of the model to generate the complete set of temperature-dependent material model parameters.

After determining the model deformation parameters for all temperatures the procedure outlined in [58] was used to calibrate initial Hayhurst-Leckie-Kachanov [58, 59] damage parameters for each temperature in the creep range using the Larson-Miller correlation developed for 316H in [4] to provide the experimental, average rupture lives. This process can be used to fit the parameters A and χ for a fixed value of parameter ϕ. In this fit, ϕ

Parameter	Units	25° C	427° C	550° C	600° C	650° C	700° C	815° C
A	MPa	32035	6269.75	3487.35	2738.64	2162.83	1722.38	1080.53
χ	-	20.619	8.214	6.939	6.526	6.144	5.777	4.917
ϕ	-	1.5	1.5	1.5	1.5	1.5	1.5	1.5

Table 3.3: Initial values of the creep damage parameters.

was kept fixed to 1.5. Table 3.3 lists these initial values of the creep damage parameters. These initial parameters were then fine-tuned by optimizing the model at each temperature against the creep data, only allowing the optimizer to alter the values of the three damage model parameters A, χ, and ϕ. The optimization method was otherwise identical to the method used to calibrate the deformation model. This process was not used to fine-tune the parameters at 25° C and 427° C as the values in Table 3.3 adequately represent negligible creep damage, as expected at this temperatures. The process was also not used to tune the 700° C and 815° C values as there were only a limited set of available creep data at these two temperatures, insufficient to constrain the three damage model parameters. The initial parameters from Table 3.3 were used with some small manual tweaks.

The damage model was superimposed on the deformation model to form the final recommended model for 316H.

3.5 Final model parameters

Table 3.4 lists the final model parameters optimized against the experimental database using the procedure described in the previous section. The odd-valued temperature control points of 427° C and 815° C were selected to match the start of the ASME high temperature range, defined by Section III, Division 5 HAA-1130 [32], and the maximum use temperature for 316H stainless steel as defined by the Section III, Division 5 allowable stress table HBB-I-14.3B. For temperatures between the control points in the table the parameters should be interpolated linearly. Note at 25° C and 427° C the creep damage parameters induce negligible creep damage, corresponding to negligible creep deformation.

A reference implementation of this model is available in the Nuclear Material model Library (NEML), maintained as open source software by Argonne National Laboratory (`https://github.com/Argonne-National-Laboratory/neml`).

If possible we recommend that the coefficient of thermal expansion be interpolated over finer increments of temperature than those provided for the mechanical properties in Table 3.4. The values of the instantaneous thermal expansion coefficient in Section II, Part D of the ASME Code can be used for this purpose [57]. This allows for a much more accurate calculation of the incremental thermal strain. However, the finite element solver would need to be able to interpolate different parameters with different schemes. The reference implementation interpolates the coefficient of thermal expansion over a very fine grid.

With the exception of the 815° C parameters the optimal values at each temperature lie well away from the bounds imposed on the optimization problem and each individual parameter follows a more-or-less smooth trajectory when plotted as a function of temperature. At 815° C tighter constraints had to be imposed on the rate sensitivity parameter n and threshold stress σ_0 in order to achieve the expected increase in rate sensitivity with

Parameter	Units	25° C	427° C	550° C	600° C	650° C	700° C	815° C
E	MPa	195,000	166,840	156,000	151,000	146,000	140,000	126,200
ν	-	0.31	0.31	0.31	0.31	0.31	0.31	0.31
α	$\frac{\text{mm/mm}}{\text{°C}}$	1.54×10^{-5}	1.96×10^{-5}	2.06×10^{-5}	2.11×10^{-5}	2.16×10^{-5}	2.17×10^{-5}	1.89×10^{-5}
η	MPa	260.21	122.00	113.52	228.09	264.89	329.67	255.39
n	-	19.419	19.011	15.842	9.2861	8.8989	7.9975	7.9000
σ_0	MPa	32.792	39.182	29.353	7.4851	16.074	13.961	12.000
Q	MPa	20.808	214.05	158.00	153.90	71.460	71.317	1.0000
b	-	7.1487	1.1807	1.0421	1.9878	4.4547	3.3879	0.01000
C_1	MPa	6111.5	7385.8	26960	15118	5028.3	1612.0	106.46
γ_1	-	416.45	480.68	506.44	309.63	89.906	12.092	2.5278
C_2	MPa	20167	7385.8	2925.6	2782.8	3980.9	6080.3	9946.9
γ_2	-	165.57	93.685	10.256	18.237	120.46	311.97	150.53
A	MPa	32035	6269.8	3767.5	2804.9	2174.0	1722.4	1180.5
χ	-	20.619	8.2140	7.2670	6.5517	6.1535	5.7778	5.1900
ϕ	-	1.5000	1.5000	1.1149	1.7100	1.2227	1.5000	1.5000

Table 3.4: Optimized parameter values at discrete temperatures.

temperature. The optimized values end up falling on these constraints, which implies that there may be a more optimal, unconstrained solution. Similarly, the optimized values of Q and b fall on the bounds for this temperature. However, these optimized values are reflecting the fact the material has nearly zero isotropic hardening at this temperature and the bound values are a reasonable way to represent this characteristic in the model. The reason for the difficulty in fitting this temperature is likely because, unlike all the other temperature control points, all the data at this temperature was collected from a single heat of material at a single laboratory (ORNL testing sponsored by the ART project). Therefore, the data did not sample the full distribution of 316H material properties and we might expect some deviation from the average material property trends expressed in the other parameter sets.

4 Model validation

Validating the final model is difficult because of the large scatter in the recorded properties of 316H. It is exceedingly unlikely that the average model will exactly match the response of any particular experiment on a random sample of 316H material. However, comparisons to the experimental database described in Chapter 2, specialized validation tests collected through ART-sponsored research, and the average material response embedded in the ASME Code demonstrate that the final model reasonably captures the average high temperature response of 316H material.

4.1 Comparison to the fit dataset

Figures 4.1-4.4 compare the model to the experimental database used to calibrated the model parameters. The figures show the results at discrete temperatures. Each figure plots a different type of response corresponding to the different standard test types:

- Figure 4.1: each plot compares the uniaxial tension test experiments (solid line) to the corresponding simulations (dashed line). The colors match between experiment and corresponding simulation. The differences in the experimental flow curves are because the tests are conducted at different strain rates and because of scatter in the 316H material properties. The model captures the average flow curve of the experimental data for all temperatures, perhaps slightly underestimating the work hardening for 650° C and underestimating the material yield stress for 815° C. At 815° C this is, again likely because the data only samples one batch of material and additional constraints were placed on the optimization problem to produce easily-interpolatable parameters.

- Figures 4.2 and 4.3: each plot compares the creep tests (solid line) to corresponding simulations (dashed line). Each plot shows results for several different values of applied stress. Figure 4.2 plots the data on a creep rate versus time diagram while Figure 4.3 plots the same data as creep strain versus time, on a semi-log scale so that all the data can be easily compared. At all temperatures the model accurately captures the initial rate of primary creep (note two lowest stress/slowest rate experimental curves for 600° C were clearly recorded incorrectly). Similarly, the model accurately captures creep rupture times, within the expected order of magnitude variation, for all temperatures. For temperatures less than 700° C the model also accurately captures the transition from primary to tertiary creep. For 700° C and 815° C the model tends to underestimate the minimum creep rate. However, these tests were for very short times and the isochronous stress-strain curve comparison below shows the model better captures the long-term, low stress creep of the material.

- Figure 4.4: each plot compares the strain-controlled cyclic (fatigue or creep-fatigue) data by plotting the maximum and, for tests where it was recorded, minimum stress in each cycle as a function of cycle count out to 300 cycles or the experimental cycles-to-failure, whichever is greater. 300 cycles is adequate to achieve a steady state response for the majority of the test data. Each plot shows all the data for the indicated temperature and so the different tests were performed for different maximum strains, strain rates, loading rates, and hold times. The model does not capture, and was not

designed to capture, the softening caused by creep-fatigue damage, most evident in the very high temperature results. However, the model does accurately represent cyclic hardening in the material as well as the saturated cyclic flow stress.

Generally, these comparisons demonstrate that the final model adequately captures the average behavior of 316H as exemplified by the complete experimental database. The model is particularly accurate for low values of strain and the long-term cyclic behavior. These are the key features to capture for a model intended for use with the ASME methods, as the total monotonic strain is limited by the Section III, Division 5 ratcheting strain criteria and, as discussed above, the cyclic results are the most important for design. Recall the cyclic test data was weighted twice as much as the monotonic data, and so the model likely compromises with a somewhat less-accurate monotonic creep and tension response in return for a more accurate representation of the cyclic response.

These comparisons are not true validation tests as the experimental data was used to calibrate the model. The next two sections discuss true validation comparisons between the model and test data not used to calibrate the model parameters.

4.2 Comparison to specialized validation tests

4.2.1 Thermomechanical tests

Figure 4.5 plots the results of a ASTM standard thermomechanical test run at Oak Ridge National Laboratory in the form of the maximum and minimum recorded stress as a function of cycle count for 50 repetitions of the thermomechanical history. The test cycled the sample between 675° and 815° C at a heating/cooling rate of 10° C/min. The sample was fully-constrained so that the total strain at any time is zero. All load on the sample is then provided by restrained thermal expansion.

Figure 4.5 also plots the results of an equivalent simulation with the inelastic model. This comparison samples not only the model coefficient of thermal expansion and response to mechanical load, but also the interpolation of the parameter set over a range of temperatures. The comparison shows that the model is somewhat less stiff than the material used in the experiment. General deviations in the flow stress might be expected based on the wide scatter in 316H mechanical properties. The model behaves reasonably by predicting very little change in the cyclic flow stress at these temperatures and conditions.

4.2.2 Detailed creep-fatigue comparison

The full stress-strain-time hysteresis data is available for the fatigue and creep-fatigue tests collected as part of the ART program. For these tests the detailed model predictions, in the form of a stress-strain hysteresis loop, can be compared to the model predictions. Unfortunately for 316H there is only a single creep-fatigue test available from the ART data at 815° C, for fully-reversed straining through a range of 1%, and with a 10 minute hold on the tensile end of the cycle. Figure 4.6 compares the model prediction to this experiment for the first 10 loading cycles, which are sufficient at this temperature to achieve a steady state response.

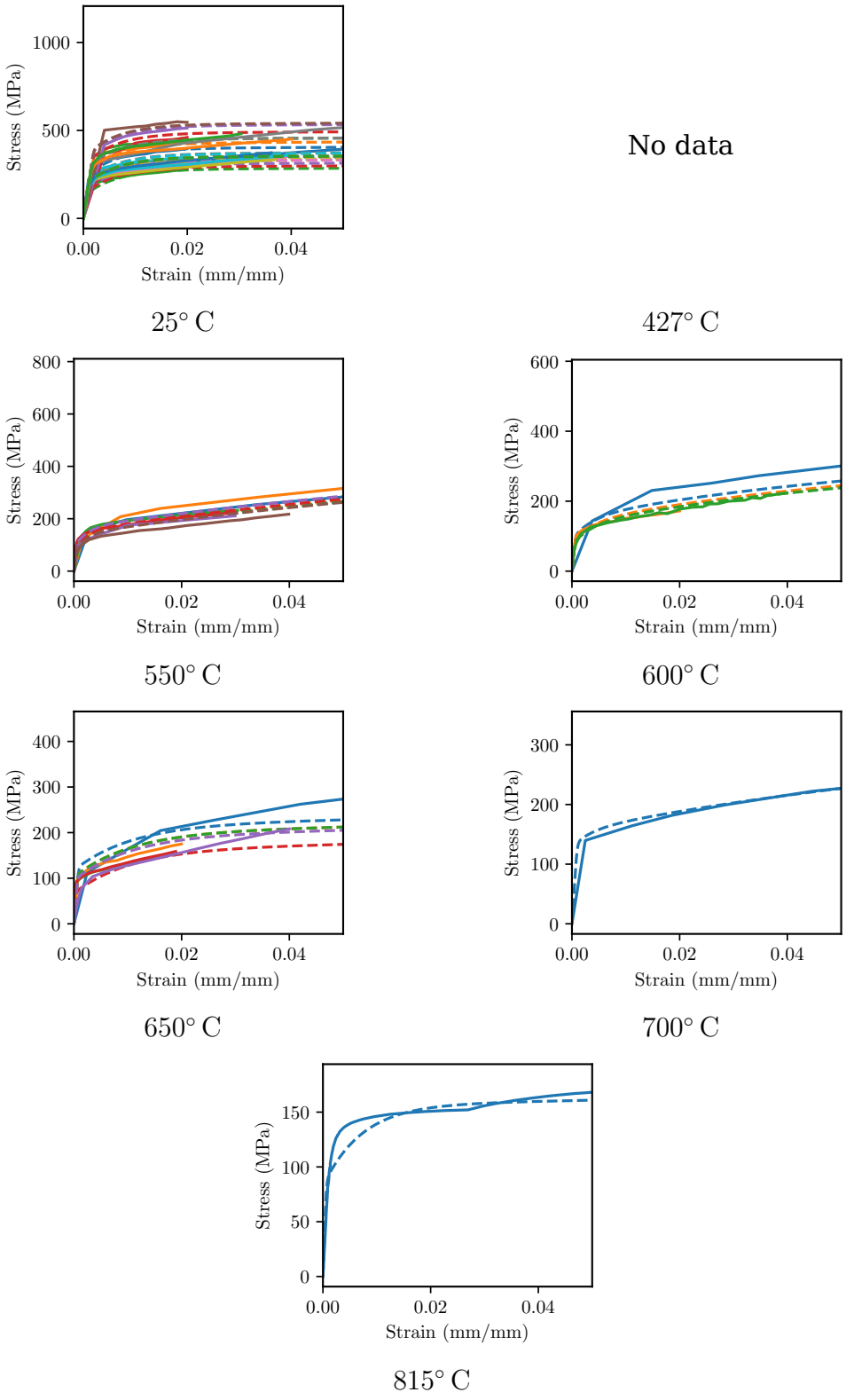

Figure 4.1: Comparison between the model (dashed line) and the experimental tension test results (solid line) for all temperatures.

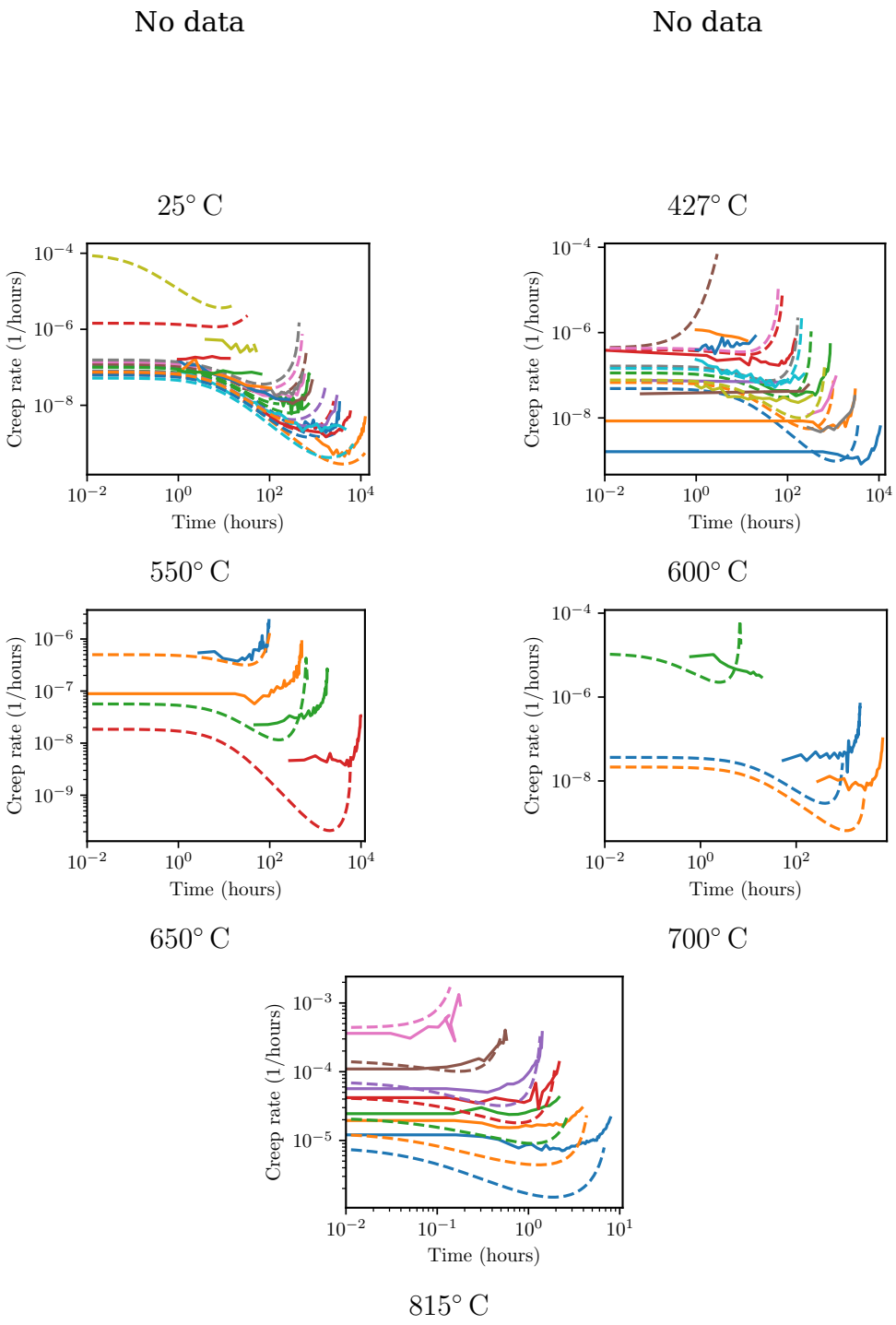

Figure 4.2: Comparison between the model (dashed line) and the experimental creep test results (solid line) for all temperatures. These figures plot the data as creep rate versus time, on a log-log scale.

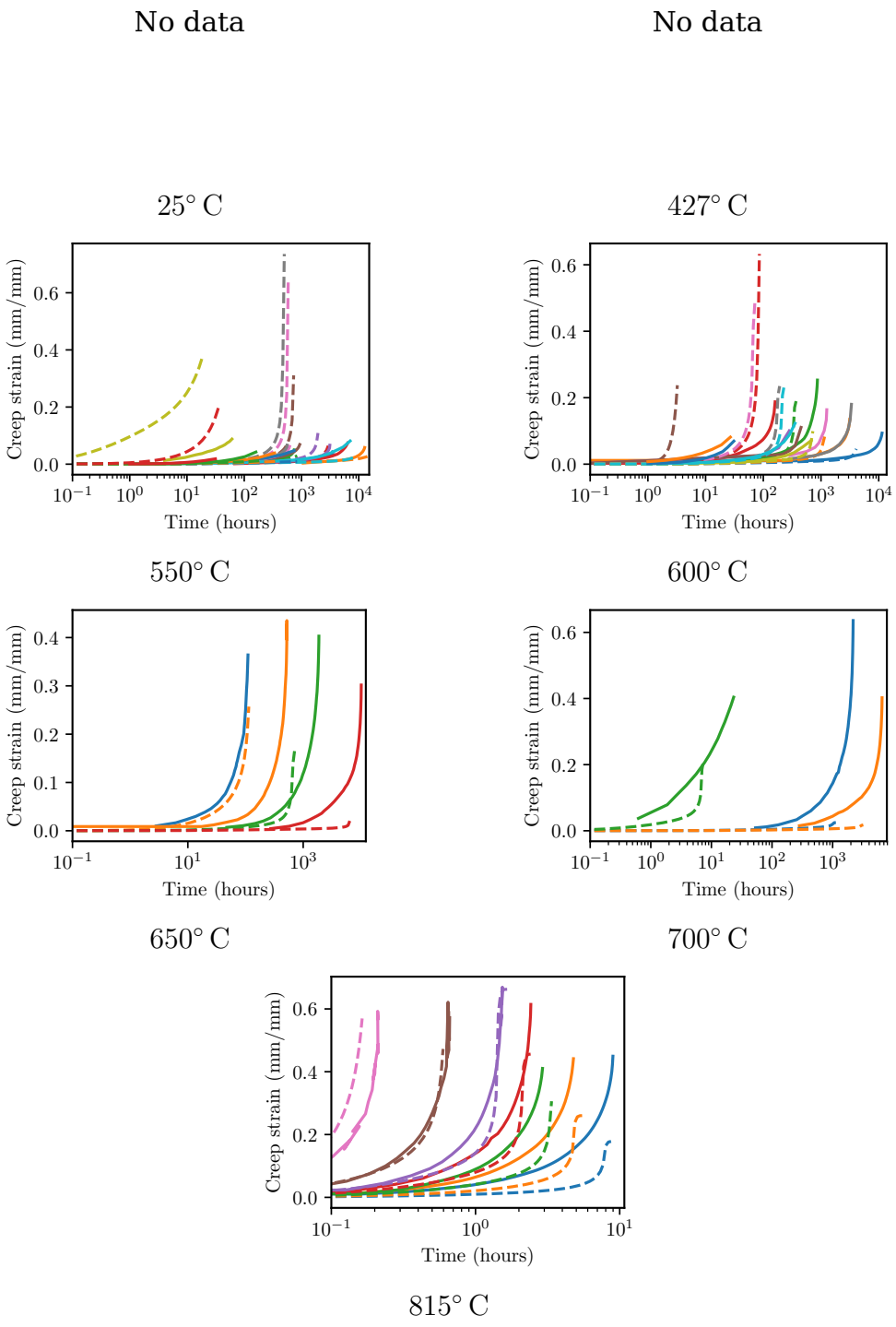

Figure 4.3: Comparison between the model (dashed line) and the experimental creep test results (solid line) for all temperatures. These figures plot the data as creep strain versus time on a semi-log scale.

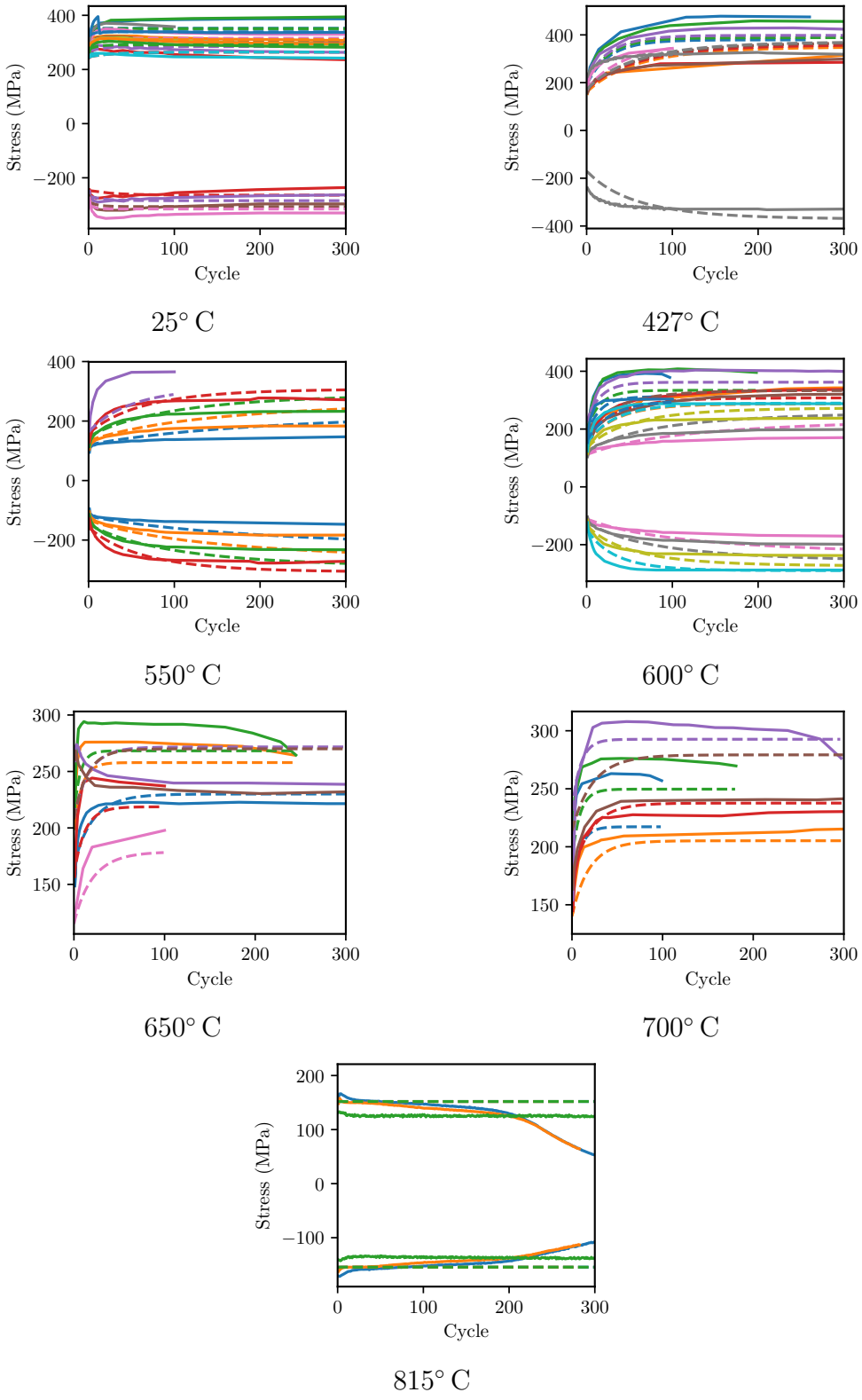

Figure 4.4: Comparison between the model (dashed line) and the experimental strain-controlled cyclic test results (solid line) for all temperatures.

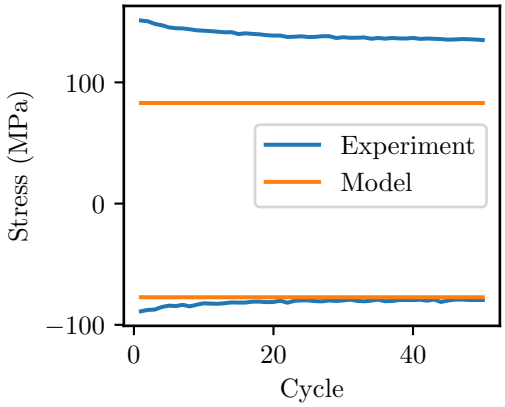

Figure 4.5: Comparison between model and experiment for a fully-restrained thermomechanical test on a sample of material.

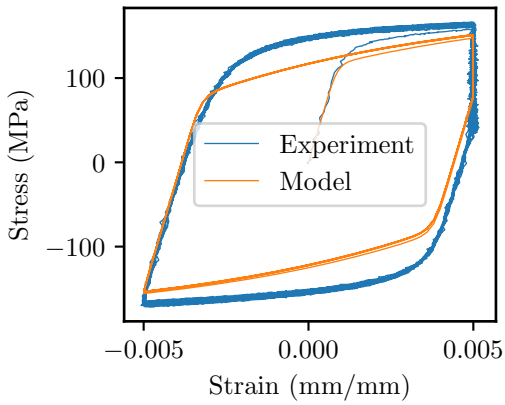

Figure 4.6: Stress-strain hysteresis loop comparison between model and an experiment at 815° C for fully-reversed straining through a range of 1% and with a 10 minute hold on the tensile end of the cycle.

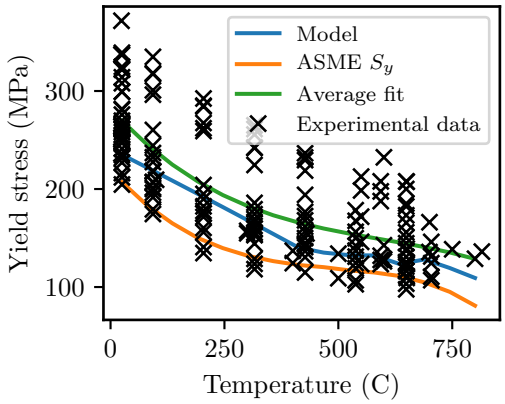

Figure 4.7: Comparison between the experimental yield stress data, the best fit to the experimental trend, the ASME values of design yield stress S_y, and the model predictions for yield stress as a function of temperature at the ASTM E-21 standard strain rate.

The model and experiment show reasonable agreement. The model represents the average response of all 316H material and the experiment essentially is a single sample of the distribution of material properties so exact correspondence between the test and simulation should not be expected. The model's cyclic response is reasonable when compared to the test and could be used for high temperature design calculations.

Ideally, additional detailed comparisons of this type would be completed for a wide range of temperatures. However, as described above, full stress-strain hysteresis data is not often available because of the difficulty in reporting such data in the literature.

4.3 Comparison to average ASME monotonic properties

4.3.1 Yield stress

The ASME values of the design yield stress S_y are developed by first fitting the average yield stress as a function of temperature and then shifting that curve to match the minimum specified yield stress at room temperature. Figure4.7 compares the yield stress predicted by the model as a function of temperature, calculated at the ASTM E-21 standard strain rate, against:

1. The ASME values of S_y.
2. All the available experimental yield stress data collected near the ASTM E-21 standard strain rate.
3. The average best fit of the experimental data.

The model predicts a somewhat softer response for 316H than the average trend. However, the model predictions fall well within the experimental scatter. The model was not calibrated to the bulk of this test data – it was only calibrated against full flow curves which

make up a small subset of all the measurements of yield and ultimate stress in the experimental database. A reasonable explanation for the model's softer response is that the flow curve measurements tended to be on a particular product form that has a lower yield stress than the average. For example, flow curves on plate material compared to yield stress data from plate and bar stock would explain this shift.

4.3.2 Isochronous curves

The ASME Code tacitly endorses a uniaxial, monotonic deformation model for 316H by defining design isochronous curves in Section III, Division 5, Subpart HB, Subsection B. Note that in Division 5 the isochronous curves represent an average, rather than lower bound, material response, and so can be reasonably compared to the model predictions. These isochronous curves are simply a way to plot a standard, uniaxial, nonunified model for deformation where the total strain is decomposed into elastic, rate-independent plastic, and rate-dependent creep contributions:

$$\varepsilon = \varepsilon_e(\sigma, T) + \varepsilon_p(\sigma, T) + \varepsilon_{cr}(\sigma, T, t).$$

The deformation model specified in the current, 2019 version of the ASME Code dates to work by Blackburn [67].

Figure 4.8 compares the model predictions for uniaxial deformation to the Code model. The plots show the Code results in solid lines and the model predictions with dashed lines. From top (highest stress) to bottom (lowest stress) the results are for the hot tensile curve (deformation at zero time) and for 1, 10, 100, 1,000, 10,000, 100,000, and 300,000 hours of creep deformation. When comparing the model to the ASME data two factors should be kept in mind:

1. Both models are extrapolating data. In particular the low temperature and long time creep response in both the ASME and the viscoplastic model are extrapolated from much shorter-term experimental data. There is little evidence, if any, to demonstrate which extrapolation is more accurate.

2. The comparison is very sensitive to the selection of the hot tensile response. The Blackburn model represents a different work hardening behavior than the current model. However, Fig. 4.1 demonstrates that the current model is making reasonable predictions for the flow behavior when compared to the experimental data. The differences in the hot tensile curves can then be attributed to working with different data sets and modeling decisions.

Given the uncertainties in representing and extrapolating creep data, the two models are in reasonable agreement above 550° C. At lower temperatures the viscoplastic model predicts more creep deformation than the Blackburn model. There is no experimental data to directly validate either of these extrapolated predictions but either set of curves could reasonably be used for engineering design.

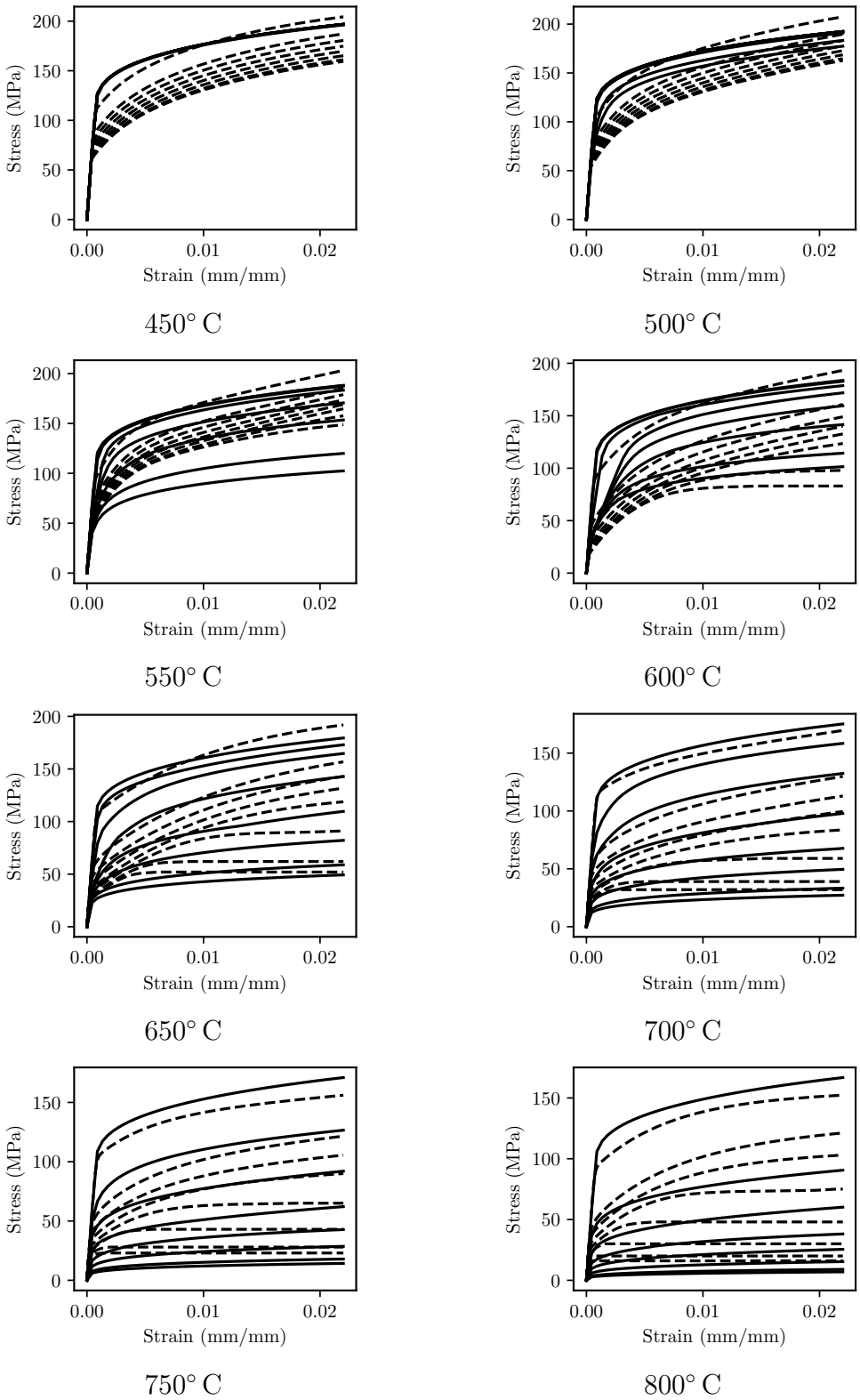

Figure 4.8: Comparison between the ASME isochronous curves (solid lines) and the model predictions (dashed lines). From top to bottom the curves shown are the 0 (hot tensile), 1, 10, 100, 1,000, 10,000, 100,000, and 300,000 hour isochronous curves.

5 Conclusions

Appendix A restates the mathematical definition of the model in the form of an ASME Code proposal. The 316H model will be integrated with general guidance on design by inelastic analysis and a previously-developed model for Grade 91 steel and proposed for incorporation in the ASME Code as a nonmandatory appendix to Section III, Division 5. This report will serve as the basis of a background document supporting balloting in the relevant ASME Codes and Standards committees. Balloting should begin at the Code Week following the completion of this report and should take around four Code Weeks to complete, barring serious technical concerns raised during the balloting process. This is the first time an inelastic model will be balloted in the Section III high temperature working groups and so this initial ballot will also provide the ballot model for subsequent work on inelastic constitutive models.

In addition to the development of the 316H model for implementation in the ASME Code, this report also described the development of a new, gradient-based method of fitting inelastic models to data. This method is broadly applicable to multiple types of materials and different types of constitutive models. The process, and the software tools developed to support it, will be used to support the calibration of additional deformation models for high temperature reactor structural materials.

The sensitivity information made available through the new method is valuable information in understanding the uncertainties in the model predictions, in addition to providing an efficient way to fit a model to the average material response. Future work might concentrate on using the tool set to develop methods of calibrating not only average inelastic models but also understanding the expected variation in material response given the experimental distribution in material properties. Ideally, engineering methods could be developed to associated probabilities with particular constitutive responses, to help designers understand the uncertainty in their designs. There will be several challenges to applying probabilistic design methods to nonlinear, history-dependent high temperature deformation and failure. These challenges include applying uncertainty quantification to nonlinear models calibrated with (relatively) sparse data, quantifying uncertainties when extrapolating from short-term experimental data, propagating uncertainties through component models undergoing cyclic loading, where simulation times are necessarily long due to the required time integration, and providing engineers with simplified probabilistic methods can be used for engineering design.

A Proposed addition to the ASME Code

HBB-Z-1322 316 SS

The reference model for 316SS is defined by the following equations in rate form. The implementation of the model will require selecting an appropriate numerical time integration scheme. Table HBB-Z-1322-1 lists the notation used in HBB-Z-1322. Variables indicated by "rate" in the "Type" column comprise the rate-form definition of the model. Variables indicated by "history" in the "Type" column are internal history variables maintained by the model. Variables indicated by "parameter" in the "Type" column are model parameters, defined in Table HBB-Z-1322-2. Variables indicated by "descriptive" in the "Type" column are neither model parameters nor history variables and are used in the model exposition.

This model uses metric units with temperatures in Celsius and the definition here assumes a small strain constitutive response. To fully-define the model requires a definition of the stress rate and the rate of each history variable. An implementation then numerically integrates the rate form definition. The model as presented here is given in strain-space, where the input is the strain, strain rate, temperature, and temperature rate and the output is the stress rate. All logarithms in the subsequent definitions are natural logarithms.

Table HBB-Z-1322-1

Variable	Description	Type
$\boldsymbol{\sigma}$	Stress	descriptive
$\dot{\boldsymbol{\sigma}}$	Stress rate	rate
$\dot{\boldsymbol{\varepsilon}}$	Strain rate	descriptive
T	Temperature in Celsius	descriptive
$\dot{T}$	Temperature rate	descriptive
E	Young's modulus	parameter
ν	Poisson's ratio	parameter
$\boldsymbol{C}$	Elasticity tensor	descriptive
α	Coefficient of thermal expansion	parameter
$\boldsymbol{I}$	Identity tensor	descriptive
$\dot{\boldsymbol{\varepsilon}}_{inelastic}$	Inelastic strain rate	descriptive
$\dot{\gamma}$	Plastic multiplier	descriptive
n	Rate sensitivity exponent	parameter
η	Viscoplastic fluidity	parameter
σ_0	Threshold stress	parameter
σ_1	Isotropic hardening	descriptive
$\boldsymbol{x}$	Kinematic hardening	descriptive
$\dot{\sigma}_1$	Isotropic hardening rate	rate
δ	Voce parameter	parameter
Q	Voce saturation stress	parameter
$\boldsymbol{x}_1$	First backstress	descriptive
$\dot{\boldsymbol{x}}_1$	First backstress rate	rate
$\boldsymbol{x}_2$	Second backstress	descriptive
$\dot{\boldsymbol{x}}_2$	Second backstress rate	rate
C_1	First Chaboche hardening parameter	parameter
γ_1	First Chaboche dynamic recovery parameter	parameter
C_1	Second Chaboche hardening parameter	parameter
γ_1	Second Chaboche dynamic recovery parameter	parameter
$\boldsymbol{s}$	Stress deviator	descriptive
$\boldsymbol{\omega}$	Damage rate	descriptive
A	Damage model prefactor	parameter
χ	Damage model exponent	parameter
φ	Damage model exponent	parameter

The model is defined by the rate equations:

$$\dot{\boldsymbol{\sigma}} = (1-\omega)\boldsymbol{C}\colon\left(\dot{\boldsymbol{\varepsilon}} - \dot{\boldsymbol{\varepsilon}}_{inelastic} - \alpha\dot{T}\boldsymbol{I}\right)$$

$$\dot{\sigma}_1 = \delta(\sigma_1 - Q)\dot{\gamma}$$

$$\dot{\boldsymbol{x}}_1 = \left(\frac{2}{3}C_1\frac{\partial f}{\partial \boldsymbol{\sigma}} - \sqrt{\frac{2}{3}}\gamma_1\boldsymbol{x}_1\right)\dot{\gamma}$$

$$\dot{\boldsymbol{x}}_2 = \left(\frac{2}{3}C_2\frac{\partial f}{\partial \boldsymbol{\sigma}} - \sqrt{\frac{2}{3}}\gamma_2\boldsymbol{x}_2\right)\dot{\gamma}$$

$$\dot{\omega} = \frac{\left(\frac{\sqrt{\frac{3}{2}\boldsymbol{s}:\boldsymbol{s}}}{A}\right)^{\chi}}{(1-\omega)^{\varphi}}$$

where : indicates double contraction of the elasticity tensor on the strain rate. The elasticity tensor is isotropic, defined by the temperature-dependent values of E and ν given in Section II, Part D (Metric) Tables TM-1 and PRD. Section II, Part D (Metric) Table TE-1 defines the values of the temperature dependent instantaneous coefficient of thermal expansion.

The flow surface is

$$f = \sqrt{\frac{3}{2}(\boldsymbol{s}-\boldsymbol{x}):(\boldsymbol{s}-\boldsymbol{x})} - \sqrt{\frac{2}{3}}(\sigma_0 + \sigma_1)$$

where $\boldsymbol{s}$ is the stress deviator

$$\boldsymbol{s} = \boldsymbol{\sigma} - \frac{1}{3}\mathrm{tr}\,\boldsymbol{\sigma}\,\boldsymbol{I}$$

with tr indicating the trace of a tensor, the double-brackets indicating $\|\boldsymbol{Y}\| = \sqrt{\boldsymbol{Y}:\boldsymbol{Y}}$ with : indicating double contraction on the tensor, and

$$\boldsymbol{x} = \boldsymbol{x}_1 + \boldsymbol{x}_2$$

The inelastic strain rate is

$$\dot{\boldsymbol{\varepsilon}}_{inelastic} = \dot{\gamma}\frac{\partial f}{\partial \boldsymbol{\sigma}}$$

$$\dot{\gamma} = \sqrt{\frac{3}{2}}\left\langle\frac{f}{\sqrt{2/3}\eta}\right\rangle^{n}$$

with $\langle\ \ \rangle$ the Macaulay brackets.

These equations completely define the model. Table HBB-Z-1322-2 defines the temperature dependent material model parameters. Values should be interpolated linearly between the temperatures provided in the table.

Table HBB-Z-1322-2

Parameter	Units	25℃	427℃	550℃	600℃	650℃	700℃	815℃
η	MPa	260.21	122.00	113.52	228.09	264.89	329.67	255.39
n	-	19.419	19.011	15.842	9.2861	8.8989	7.9975	7.9000
σ_0	MPa	32.792	39.182	29.353	7.4851	16.074	13.961	12.000
Q	MPa	20.808	214.05	158.00	153.90	71.460	71.317	1.0000
δ	-	7.1487	1.1807	1.0421	1.9878	4.4547	3.3879	0.010000
C_1	MPa	6111.5	7385.8	26960	15118	5028.3	1612.0	106.46
γ_1	-	416.45	480.68	506.44	309.63	89.906	12.092	2.5278
C_2	MPa	20167	7385.8	2925.6	2782.8	3980.9	6080.3	9946.9
γ_2	-	165.57	93.685	10.256	18.25337	120.46	311.97	150.53
A	MPa	32035	6269.8	3767.5	2804.9	2174.0	1722.4	1180.5
χ	-	20.619	8.2140	7.2670	6.5517	6.1535	5.7778	5.1900
φ	-	1.5000	1.5000	1.1149	1.7100	1.2227	1.5000	1.5000

Acknowledgments

The research was sponsored by the U.S. Department of Energy, under Contract No. DE-AC02-06CH11357 with Argonne National Laboratory, managed and operated by UChicago Argonne LLC. Programmatic direction was provided by the Office of Nuclear Reactor Deployment of the Office of Nuclear Energy. The authors gratefully acknowledge the support provided by Sue Lesica, Federal Manager, Advanced Materials, Advanced Reactor Technologies (ART) Program, and Gerhard Strydom of Idaho National Laboratory, National Technical Director, ART Gas-Cooled Reactors Campaign.

Bibliography

[1] J. B. Kim, H. Y. Lee, C. G. Park, and J. H. Lee, "Creep-fatigue test of a SA 316SS structure and comparative damage evaluations based upon elastic and inelastic approaches," *International Journal of Pressure Vessels and Piping*, vol. 85, no. 8, pp. 550–556, 2008.

[2] V. K. Sikka, B. L. P. Booker, M. K. Booker, and J. W. McEnerney, "Tensile and Creep Data on Type 316 Stainless Steel," tech. rep., Oak Ridge National Laboratory, OSTI 711239, 1980.

[3] "Personal communication with Y. Wang."

[4] M. Sengupta and J. E. Nestell, "Correct and Extend Allowable Stress Values for 304 and 316 Stainless Steel," tech. rep., ASME Standards Technology, LLC STP-NU-063, New York, 2013.

[5] M. D. Mathew, K. Laha, and V. Ganesan, "Improving creep strength of 316L stainless steel by alloying with nitrogen," *Materials Science and Engineering A*, vol. 535, pp. 76–83, 2012.

[6] S. Holmström, R. Pohja, A. Nurmela, P. Moilanen, and P. Auerkari, "Creep and creep-fatigue behaviour of 316 stainless steel," *Procedia Engineering*, vol. 55, pp. 160–164, 2013.

[7] Y. Q. Wang, M. W. Spindler, C. E. Truman, and D. J. Smith, "Critical analysis of the prediction of stress relaxation from forward creep of Type 316H austenitic stainless steel," *Materials and Design*, vol. 95, pp. 656–668, 2016.

[8] T. Asayama, Y. Nagae, T. Wakai, M. Inoue, T. Kaito, S. Otuka, N. Kawasaki, and M. Morishita, "Development of Structural Materials for JSFR," in *International Conference on Fast Reactors and Related Fuel Cycles*, 2009.

[9] A. K. Dhalla, "Recommended practices in elevated temperature design: a compendium of breeder reactor experiences (1970-1987): Volume III - Inelastic analysis," Tech. Rep. 366, 1991.

[10] M. C. Messner, R. I. Jetter, and T.-L. Sham, "Establishing Temperature Upper Limits for the ASME Section III, Division 5 Design by Elastic Analysis Methods," in *ASME 2018 Pressure Vessels and Piping Conference*, pp. V01BT01A016–V01BT01A016, 2018.

[11] M. C. Messner and T.-L. Sham, "Development of ASME Division 5 Code proposal on temperature limits for simplified design methods," tech. rep., Argonne National Laboratory, ANL-ART-132, OSTI 146672, 2018.

[12] ASTM International, "E 21-09: Standard Test Methods for Elevated Temperature Tension Tests of Metallic Materials," 2009.

[13] K. Kanazawa and S. Yoshida, "Creep and Fatigue in Elevated Temperature Applications," *Institution of Mechanical Engineers*, vol. 1, p. C226, 1974.

[14] N. Ohno, M. Abdel-Karim, M. Kobayashi, and T. Igari, "Ratchetting characteristics of 316FR steel at high temperature, part I: Strain-controlled ratchetting experiments and simulations," *International Journal of Plasticity*, vol. 14, no. 4-5, pp. 355–372, 1998.

[15] T. H. Hyde, "Creep of 316 stainless steel at 550 and 600C and the effects of short duration overloads on creep at 550C," *Materials at High Temperatures*, vol. 14, no. 1, pp. 27–35, 1997.

[16] S. Mohanty, W. K. Soppet, S. Majumdar, and K. Natesan, "In-air and pressurized water reactor environment fatigue experiments of 316 stainless steel to study the effect of environment on cyclic hardening," *Journal of Nuclear Materials*, vol. 473, pp. 290–299, 2016.

[17] A. Fookes, S. X. Li, D. J. Smith, and M. W. Spindler, "Stress Relaxation during Dwells for Creep and Fatigue Cycling of Type 316H Stainless Steel at 550Â°C," in *2nd International ECCC Conference*, 2009.

[18] C. Albertini, M. Montagnani, E. V. Pizzinato, and A. Rodis, "Comparison of the equivalent flow curves in tension and shear at low and high strain rate for AISI 316 and ARMCO iron," in *Transactions of the 11th international conference on structural mechanics in reactor technology*, pp. 103–108, 1991.

[19] J. P. Hammond and V. K. Sikka, "Heat-to-heat variations of total strain (to 5%) at discrete stress levels in types 316 and 304 stainless steel from 24 to 316 C," tech. rep., Oak Ridge National Laboratory, ORNL/NUREG/TM-57, 1976.

[20] Y. Takahashi, H. Shibamoto, and K. Inoue, "Long-term creep rupture behavior of smoothed and notched bar specimens of low-carbon nitrogen-controlled 316 stainless steel (316FR) and their evaluation," *Nuclear Engineering and Design*, vol. 238, no. 2, pp. 310–321, 2008.

[21] J. Horak, V. Sikka, and D. Raske, "Review of mechanical properties and microstructures of Types 304 and 316 stainless steel after long-term aging," tech. rep., Oak Ridge National Laboratory, OSTI 6270710, 1983.

[22] J. H. Zhu, D. Boerman, and G. Piatti, "Strength of the AISI 316 Stainless Steel Above 800 C," in *Transactions of the 7th International Conference on Structural Mechanics in Reactor Technology*, pp. 507–514, 1983.

[23] M. Mizuno, "Uniaxial ratchetting of 316FR steel at room temperature – Part I: experiments," *Journal of Engineering Materials and Technology*, vol. 122, no. January 2000, pp. 29–34, 2000.

[24] J. H. Yoon, Y. C. Kim, S. Hong, G. H. Koo, and B. S. Lee, "Inelastic cyclic deformation behaviors of type 316H stainless steel for reactor pressure vessel of sodium-cooled fast reactor at elevated temperatures," *Journal of Korean Institute of Metals and Materials*, vol. 53, no. 10, pp. 681–687, 2015.

[25] D. S. Wood, A. B. Baldwin, T. J. Sarbutts, and K. Williamson, "The low temperature deformation behavior of type 316 steel," in *Materials for Nuclear Reactor Core Applications*, pp. 2–7, 1987.

[26] T. H. Hyde, "Anomalous creep behaviour of 316 stainless steel at 550C," *High Temperature Technology*, vol. 4, no. 1, pp. 25–29, 1986.

[27] M. T. Whittaker, M. Evans, and B. Wilshire, "Long-term creep data prediction for type 316H stainless steel," *Materials Science and Engineering A*, vol. 552, pp. 145–150, 2012.

[28] T. S. DeSisto and F. L. Carr, "Low temperature mechanical properties of 300 series stainless steels and titanium," tech. rep., Watertown Arsenal Laboratories, WAL-TR-323.4/1, 1961.

[29] R. Hormozi, F. Biglari, and K. Nikbin, "Experimental study of type 316 stainless steel failure under LCF/TMF loading conditions," *International Journal of Fatigue*, vol. 75, pp. 153–169, 2015.

[30] A. G. Youtsos, J. Donea, and G. Verzeletti, "Viscoplastic behavior of stainless steels AISI 316L and 316H," *Acta Mechanica*, vol. 76, pp. 161–187, 1989.

[31] F. Yoshida, M. Kobayashi, K. Tsukimori, T. Uno, Y. Fukuda, T. Igari, and T. Inoue, "Inelastic Analysis of Material Ratchetting of 316FR at Varying Temperature – Results of Benchmark Project (B) by JSMS," in *Transactions of the 14th International Conference on Structural Mechanics in Reactor Technology*, pp. 221–228, 1997.

[32] American Society of Mechanical Engineers, "Section III, Division 5," in *ASME Boiler and Pressure Vessel Code*, 2017.

[33] J. M. Corum, "Evaluation of Inelastic Analysis Methods," in *Transactions of the 4th International Conference on Structural Mechanics in Reactor Technology*, 1977.

[34] K. C. Liu, "Room-Temperature Elastic-Plastic Response of Thin-Walled Tubes Subjected to Nonradial Combinations of Axial and Torsional Loadings," in *Pressure Vessel and Piping: Verification and Qualification of Inelastic Analysis Computer Programs* (J. M. Corum and W. B. Wright, eds.), New York: ASME Press, 1975.

[35] C. E. Pugh, "Constitutive Equations for Creep Analysis of LMFBR Components," in *Advances in Design for Elevated Temperature Environment* (S. Y. Zamrik and R. I. Jetter, eds.), New York: ASME Press, 1975.

[36] C. E. Pugh and D. N. Robinson, "Some Trends in Constitutive Equation Model Development for High-Temperature Behavior of Fast-Reactor Structural Alloy," *Nuclear Engineering and Design*, vol. 48, pp. 269–276, 1978.

[37] C. E. Pugh and D. N. Robinson, "Constitutive Equations for Meeting Elevated Temperature Design Needs," in *Pressure Vessel and Piping Design Technology, A Decade of Progress*, pp. 7–10, 1981.

[38] Y. P. Gong, C. J. Hyde, W. Sun, and T. H. Hyde, "Determination of material properties in the Chaboche unified viscoplasticity model," *Proceedings of the Institution of Mechanical Engineers, Part L: Journal of Materials: Design and Applications*, vol. 224, no. 1, pp. 19–29, 2010.

[39] K. Tokuda, T. Sasaki, K. Yoshida, N. Ohno, and T. Shimada, "Creep-Fatigue Life Prediction of 316H Stainless Steel by Utilizing Non-Unified Constitutive Model," *Procedia Structural Integrity*, vol. 13, pp. 1873–1878, 2018.

[40] J. L. Chaboche and D. Nouailhas, "A unified constitutive model for cyclic viscoplasticity and its applications to various stainless steels," *Journal of Engineering Materials and Technology*, vol. 111, pp. 424–430, 1989.

[41] H. Y. Lee, J. B. Kim, and J. H. Lee, "Thermal ratchetting deformation of a 316L stainless steel cylindrical structure under an axial moving temperature distribution," *International Journal of Pressure Vessels and Piping*, vol. 80, no. 1, pp. 41–48, 2003.

[42] W. Chen, T. Kitamura, and M. Feng, "Creep and fatigue behavior of 316L stainless steel at room temperature: Experiments and a revisit of a unified viscoplasticity model," *International Journal of Fatigue*, vol. 112, no. March, pp. 70–77, 2018.

[43] M. Dalla Palma, "Modelling of cyclic plasticity for austenitic stainless steels 304L, 316L, 316L(N)-IG," *Fusion Engineering and Design*, vol. 109-111, pp. 20–25, 2016.

[44] X. Yang, "A viscoplastic model for 316L stainless steel under uniaxial cyclic straining and stressing at room temperature," *Mechanics of Materials*, vol. 36, no. 11, pp. 1073–1086, 2004.

[45] N. Ohno and J.-D. Wang, "Kinematic hardening rules with critical state of dynamic recovery, part I: formulation and basic features for ratchetting behavior," *International Journal of Plasticity*, vol. 9, no. 3, pp. 375–390, 1993.

[46] N. Ohno and J.-D. Wang, "Kinematic hardening rules with critical state of dynamic recovery, part II: Application to experiments of ratchetting behavior," *International Journal of Plasticity*, vol. 9, no. 3, pp. 391–403, 1993.

[47] E. Krempl, "Models of viscoplasticity some comments on equilibrium (back) stress and drag stress," *Acta Mechanica*, vol. 69, no. 1-4, pp. 25–42, 1987.

[48] E. Krempl, "Creep-Plasticity Interaction," in *Creep and Damage in Materials and Structures* (H. Altenbach and J. J. Skrzypek, eds.), pp. 285–348, Springer-Verlag, 1999.

[49] M. C. Liu and E. Krempl, "A uniaxial viscoplastic model based on total strain and overstress," *Journal of the Mechanics and Physics of Solids*, vol. 27, no. 5-6, pp. 377–391, 1979.

[50] J. L. Chaboche and G. Cailletaud, "On the calculation of structures in cyclic plasticity or viscoplasticity," *Computers and Structures*, vol. 23, no. 1, pp. 23–31, 1986.

[51] J. L. Chaboche, "Time-independent constitutive theories for cyclic plasticity," *International Journal of Plasticity*, vol. 2, no. 2, pp. 149–188, 1986.

[52] J. Chaboche, "Constitutive equations for cyclic plasticty and cyclic viscoplasticity," *International Journal of Plasticity*, vol. 5, pp. 247–302, 1989.

[53] J. L. Chaboche, "On some modifications of kinematic hardening to improve the description of ratchetting effects," *International Journal of Plasticity*, vol. 7, no. 7, pp. 661–678, 1991.

[54] J. L. Chaboche and G. Cailletaudb, "Integration methods for complex plastic constitutive equations," *Computational Methods in Applied Mechanics and Engineering*, vol. 133, no. 95, pp. 125–155, 1996.

[55] J.-L. Chaboche, "Thermodynamic formulation of constitutive equations and application to the viscoplasticity and viscoelasticity of metals and polymers," *International Journal of Solids and Structures*, vol. 34, no. 18, pp. 2239–2254, 1997.

[56] J. L. Chaboche, "A review of some plasticity and viscoplasticity constitutive theories," *International Journal of Plasticity*, vol. 24, pp. 1642–1693, oct 2008.

[57] American Society of Mechanical Engineers, "Section II, Part D (Metric)," in *ASME Boiler and Pressure Vessel Code*, 2015.

[58] F. A. Leckie and D. R. Hayhurst, "Creep rupture of structures," *Proceedings of the Royal Society A: Mathematical, Physical and Engineering Sciences*, vol. 340, pp. 323–347, 1974.

[59] L. M. Kachanov, "On the creep fracture time," *Izv Akad, Nauk USSR Otd Tech*, vol. 8, pp. 23–31, 1958.

[60] M. C. Messner, V.-T. Phan, and T.-L. Sham, "FY17 Status Report on the Initial Development of a Constitutive Model for Grade 91 Steel," tech. rep., Argonne National Laboratory ANL-ART-93 OSTI 136734, 2017.

[61] M. C. Messner, V.-T. Phan, and T.-L. Sham, "A Unified Inelastic Constitutive Model for the Average Engineering Response of Grade 91 Steel," in *Proceedings of the 2018 ASME Pressure Vessels and Piping Conference*, PVP2018-84104, 2018.

[62] M. C. Messner, V.-T. Phan, and T.-L. Sham, "Development of Grade 91 inelastic model for incorporation in ASME Division 5," tech. rep., Argonne National Laboratory ANL-ART-137 OSTI 146678, 2018.

[63] M. Gen and L. Lin, "Genetic Algorithms," in *Wiley Encylopedia of Computer Science and Engineering*, pp. 1–15, 2007.

[64] S. G. Nash, "A survey of truncated-Newton methods," *Journal of Computational and Applied Mathematics*, vol. 124, pp. 45–59, 2000.

[65] D. Solow, "Linear and Nonlinear Programming," in *Wiley Encyclopedia of Computer Science and Engineering*, 2007.

[66] A. Wachter and L. Biegler, *On the implementation of an interior-point filter line-search algorithm for large-scale nonlinear programming*, vol. 106. 2006.

[67] L. D. Blackburn, "Isochronous Stress-Strain Curves for Austenitic Stainless Steels," in *The Generation of Isochronous Stress-Strain Curves* (A. O. Schaefer, ed.), pp. 15–48, The American Socieity of Mechanical Engineers, 1972.

Applied Materials Division
Argonne National Laboratory
9700 South Cass Avenue, Bldg. 212
Argonne, IL 60439

www.anl.gov